Published in final edited form as:
JACC Cardiovasc Imaging. 2011 September ; 4(9): 1022–1039. doi:10.1016/j.jcmg.2011.03.020.

Intravascular Optical Imaging Technology for Investigating the Coronary Artery

Melissa J. Suter, PhD[*,†], **Seemantini K. Nadkarni, PhD**[*,‡], **Giora Weisz, MD**[§], **Atsushi Tanaka, MD, PhD**[*,‡], **Farouc A. Jaffer, MD, PhD**[*,‖], **Brett E. Bouma, PhD**[*,‡,¶], and **Guillermo J. Tearney, MD, PhD**[*,¶,#]

[*]Wellman Center for Photomedicine, Massachusetts General Hospital, Harvard Medical School, Boston, Massachusetts

[†]Pulmonary and Critical Care Unit, Massachusetts General Hospital, Harvard Medical School, Boston, Massachusetts

[‡]Department of Dermatology, Massachusetts General Hospital, Harvard Medical School, Boston, Massachusetts

[§]Center for Interventional Vascular Therapy, New York-Presbyterian Hospital, Columbia University, and Cardiovascular Research Foundation, New York, New York

[‖]Cardiovascular Research Center, Cardiology Division, and Center for Molecular Imaging Research, Massachusetts General Hospital, Harvard Medical School, Boston Massachusetts

[¶]Harvard-MIT Division of Health Sciences and Technology, Cambridge, Massachusetts

[#]Department of Pathology, Massachusetts General Hospital, Harvard Medical School, Boston, Massachusetts

Abstract

There is an ever-increasing demand for new imaging methods that can provide additional information about the coronary wall to better characterize and stratify high-risk plaques, and to guide interventional and pharmacologic management of patients with coronary artery disease. While there are a number of imaging modalities that facilitate the assessment of coronary artery pathology, this review paper focuses on intravascular optical imaging modalities that provide information on the microstructural, compositional, biochemical, biomechanical, and molecular features of coronary lesions and stents. The optical imaging modalities discussed include angioscopy, optical coherence tomography, polarization sensitive-optical coherence tomography, laser speckle imaging, near-infrared spectroscopy, time-resolved laser induced fluorescence spectroscopy, Raman spectroscopy, and near-infrared fluorescence molecular imaging. Given the wealth of information that these techniques can provide, optical imaging modalities are poised to play an increasingly significant role in the evaluation of the coronary artery in the future.

Keywords

intracoronary; optical diagnostics; optical imaging

Reprint requests and correspondence: Dr. Guillermo J. Tearney, Massachusetts General Hospital, Wellman Center for Photomedicine, 40 Blossom Street, BAR 701, Boston, Massachusetts 02114. gtearney@partners.org.

All other authors have reported they have no relationships relevant to the contents of this paper to disclose.

Despite widespread efforts toward its detection and treatment, acute cardiovascular events are still the leading cause of death in the Western world (1). The rupture of an unstable coronary atherosclerotic plaque frequently precedes a majority of acute cardiovascular events (2,3). The strong association between atherosclerotic plaque stability and the incidence of acute events has warranted the development of diagnostic techniques to identify rupture-prone plaques. The quest for detecting unstable plaques has been evolving over the years, from measuring luminal stenoses using angiography to more advanced evaluation of the vessel wall.

There is compelling evidence suggesting that the mechanisms intrinsic to coronary lesions that lead to acute thrombosis are multi-factorial, involving a complex interplay between structural, compositional, biochemical, biomechanical, cellular, and molecular processes in the vessel wall, as well as complex humoral factors. Autopsy studies suggest the typical hallmarks of the majority of unstable plaques are the presence of a thin fibrous cap, a large compliant necrotic core, and activated macrophages near the fibrous cap (4,5). Plaque instability is influenced by the proteolysis of fibrous cap collagen by matrix metalloproteinases released by activated macrophages and apoptosis of intimal smooth muscle cells (SMC), which impede collagen synthesis (6–8). Mediated by endothelial production of nitric oxide, transforming growth factor-β, and plasmin, this dynamic imbalance between collagen synthesis and degradation causes a net reduction in collagen content and a mechanical weakening of the fibrous cap (9). A recent study suggests that increased collagenase expression yields thinner collagen fibers with disorganized fiber orientation, which may be associated with decreased mechanical stability (10). Finite element studies have suggested that rupture of the fibrous cap is greatly affected by regions of high biomechanical stress (11–13). The morphology and mechanical properties of the atheroma affect stress distributions, (14,15), and plaque rupture frequently occurs in focal regions of high stress concentrations caused by large differences in the intrinsic mechanical properties of the fibrous cap and lipid pool (5,11,15–17). The cumulative effect of these multiple factors compromises the mechanical stability of the plaque, resulting in an elevated risk of rupture (11,18,19). Since multiple factors are involved in the process of atherogenesis leading to plaque rupture, diagnostic techniques that provide synergistic information on these multiple determinants may be required to prospectively detect unstable or “vulnerable” coronary plaques.

Coronary stenting during percutaneous coronary intervention (PCI) has become the standard of care for symptomatic and flow-limiting coronary artery disease. Bare-metal stents (BMS) diminish the elastic recoil of angioplasty to maintain lumen patency, but have been limited by restenosis caused by aggressive neointimal hyperplasia, therefore requiring repeat PCI in a significant proportion of patients. Although recently introduced drug-eluting stents (DES) have mitigated restenosis by inhibiting smooth-muscle cell proliferation, therapy of coronary lesions by current DES is accompanied by the need for extended dual antiplatelet therapy regimens to avoid late stent thrombosis (20–23). As a result, there is substantial interest in developing ways to assess stent healing in vivo to guide the intensity and duration of the pharmacological management of patients who were treated with DES as well as to evaluate next-generation platforms, like stents that promote re-endothelialization, and bioabsorbable stents.

Intravascular optical diagnostic techniques have provided new options for the evaluation of the various factors associated with atherosclerosis, plaque stability, and treatment of coronary artery disease. These diagnostic techniques measure one or more of the processes that occur when the light interacts with the tissue including the reflectance, refraction, scattering, or absorption and re-emission of the incident light (Fig. 1). Angioscopy allows direct visualization of the luminal artery surface (24); optical coherence tomography (OCT)

provides high-resolution cross-sectional images of plaque microarchitecture (25), stent placement (26–28), apposition (26,29–31), and strut coverage (32–36); polarization sensitive (PS)-OCT provides a measure of tissue birefringence that may be related to collagen and SMC content (37); laser speckle imaging (LSI) (38) allows the evaluation of biomechanical factors; optical spectroscopic techniques provide methods to evaluate biochemical factors related to plaque stability (39); and near-infrared fluorescence (NIRF) opens up the possibility of labeling and identifying individual molecules within the artery wall (40). Attractive properties of optical imaging modalities are that they are nondestructive, they are amenable to implementation using flexible small diameter fiber-optic catheters, and they may potentially be combined to allow simultaneous measurements of the multiple types of plaque features (41,42). These optical imaging catheters can be easily used in the clinical management of patients during coronary angiography and percutaneous intervention.

Other review articles have summarized many of the common imaging modalities used for evaluating coronary arteries, covering a combination of intravascular approaches such as intravascular ultrasonography (IVUS) and optical imaging techniques, and external to the body techniques including magnetic resonance imaging, computed tomography, and positron emission tomography (43–52). This review, however, focuses on all major intravascular optical imaging modalities. While these optical imaging modalities have been in development for years, many have recently undergone significant technical improvements, as outlined in this review. Furthermore, some of these intracoronary imaging modalities have recently become, or are becoming, commercially available and have received approval by the Food and Drug Administration (FDA) for human use. In this paper, we provide an overview of all of the current intravascular optical imaging modalities, we compare and contrast the tissue properties measured by each technique, and provide a critical review of each of the imaging modalities in terms of potential current and future clinical utility.

Angioscopy

The oldest optical imaging technique employed for investigating the coronary arteries is angioscopy (24). Angioscopy is an endoscopic imaging modality that allows direct visualization of the internal surface of the coronary artery and consists of a white light source, a flexible optical fiber bundle consisting of separate illumination fibers that guide light to, and collection fibers that collect the light reflected from the artery wall, and a distal lens at the tip of the catheter to form an image with a large field of view. Studies have demonstrated that angioscopy can be used to differentiate arterial wall composition (53), including the detection of fibrous or lipid-rich plaques, plaque disruptions, thrombi, and ulcerations, to assess plaque vulnerability (54–56), the response to treatment therapies (57,58), and to evaluate stenting procedures including stent placement, and neointimal coverage of individual stent struts (59,60) (Fig. 2). While angioscopy has been demonstrated to detect plaques and thrombi that may be missed by angiography, to provide an indication of the plaque composition through quantitative color analysis (61), and to evaluate the effectiveness of coronary stenting procedures, angioscopy is restricted to imaging surface morphology. Although angioscopy is a commercially available FDA-approved optical imaging technology that has been available for many years, its use in the United States has been largely restricted to research applications rather than clinical practice. Limitations to the technology include the requirement to clear the coronary lumen of blood with the infusion of saline, the large catheter diameter that limits the evaluation to proximal segments, the inability to pass significant lesions, and the difficulties associated with accurate interpretation of the images, which therefore mandate expertise. Angioscopy is limited to surface and clot morphology, and adds little insight on deep plaque composition. In routine clinical use in the United States, there are no indications for angioscopy, and

therefore, at present, the use of angioscopy is restricted to research in highly specialized centers.

Optical Coherence Tomography

OCT is a high-resolution (<10 μm axial; 20 to 40 μm lateral resolution) imaging modality that generates cross-sectional images of tissue microstructure to penetration depths approaching 2 mm (62). The underlying concept of OCT is similar to that of ultrasonography; by measuring the delay time of optical echoes reflected from subsurface structures in biological tissues, structural information can be obtained (Fig 1). Because of the high speed of light propagation in tissue, the time delay of the returning light is measured using low-coherence interferometry.

There are 2 types of OCT, the first generation, called time domain (TD)-OCT (62,63) that has been used in patients from 2000 to the present, and second-generation frequency domain (FD)-OCT (64,65), also known as optical frequency domain imaging (OFDI) (66,67), which has advantages that currently make it the preferred technique in interventional cardiology. In TD-OCT systems, a broadband light source is split into a reference arm, directed onto a mirror, and a sample arm that directs the light into the artery wall. When the distance travelled by the light in each arm of the interferometer is within the coherence length of the source, the returning light, once recombined, will form an interference pattern. The amplitude of the detected interference pattern is subsequently mapped to a pixel intensity value corresponding to the discrete axial location, or depth, within the tissue. To generate image information for an entire axial depth profile, the reference mirror is translated, altering the optical path length of the reference arm, and hence the imaging depth inside the sample. Systematic scanning of the imaging beam across the tissue can be performed to build 2-dimensional and 3-dimensional images. For FD-OCT/OFDI, rather than utilizing a broadband light source and a mechanically translating reference arm, interference is generated using a rapidly tuned wavelength swept source and a stationary reference arm (66). Each frequency component of the detected interference signal is associated with a discrete depth location within the tissue. To generate an A-line, a technique called the Fourier transform converts the interference information to depth resolved reflectance (66).

TD-OCT has been used to image microstructural features of the artery wall in a number of post-mortem studies where the image data can be directly correlated to histopathology, the gold standard (25,68–73). These studies document the development and validation of image criteria for detecting features that correspond to tissue microstructures with high sensitivity and specificity. The detected microstructural features (Fig. 3) include macrophages (69,72), cholesterol crystals (25,71), red and white thrombus (74,75), calcium deposits (70,73), fibrous plaques (70,73), and lipid-rich plaques (70,73,76). Yabushita et al. (73) reported sensitivities and specificities of 71% to 79% and 97% to 98% for the detection of fibrous plaques, 95% to 96% and 97% for fibrocalcific plaques, and 90% to 94% and 90% to 92% for lipid-rich plaques (73). These studies have provided the foundation necessary for the interpretation of intracoronary OCT images.

Intracoronary TD-OCT in swine in vivo was performed in 2000 (77). This initial proof-of-concept study demonstrated that TD-OCT provided images of superior resolution when compared to IVUS and allowed visualization of features not seen by ultrasound, such as the intima, including intimal flaps and defects, disruptions in the media, and stent strut apposition. This study was soon followed by first-in-human demonstrations in 2002 (73,74,78,79). In the years since this initial demonstration, TD-OCT has been used extensively by a number of investigators in the clinical realm for assessing coronary plaque features (80–84), stent placement (26–28,85), apposition (26,29–31,85), stent strut coverage

(32–36,85) (Fig. 4), and thrombus (86), As for most catheter-based optical imaging modalities, it is necessary to clear blood from the imaging field of view to obtain information on the artery wall because blood scatters and attenuates light. Intracoronary OCT has been successfully demonstrated in vivo using either a flush with an optically transparent media such as saline or radiocontrast, or combined flushing with proximal balloon occlusion. While effective for displacing blood, the nonocclusive method only provides a limited view of the vessel, containing few images, and balloon occlusion may be associated with myocardial ischemia and chest pain during the procedure (87,88).

Second-generation OCT has, to a large part, solved the blood limitations of TD-OCT. In 2003, FD-OCT/OFDI (64,65,89) was shown to have a sensitivity advantage over TD-OCT. This realization led to the development of second-generation intracoronary OCT systems that perform OCT imaging at significantly higher frame rates than TD-OCT, but with superior image quality (66). When used in conjunction with a saline/radiocontrast flush and rapid helical pullback scanning of the catheter (67,90), FD-OCT/OFDI makes it practical to conduct 3-dimensional OCT imaging of long coronary artery segments without balloon occlusion (67,90). The fast pullback rate (10 to 20 mm per second) allows the injection of only a small amount of contrast media to clear the artery, therefore greatly reducing the risk of ischemia. Intracoronary OFDI was first demonstrated in vivo in swine studies in 2006, in human patients in 2008 (Fig. 5) (90), and is now poised to become a widely used imaging modality in interventional cardiology with many centers now publishing results from on-going clinical studies (91–96). In fact, intracoronary TD-OCT has been performed on thousands of coronary patients at several hundred sites around the world and, with the recent FDA approval of intracoronary FD-OCT systems in the United States, it is anticipated that these numbers will greatly increase. The use of intravascular OCT to date has been primarily investigational, and therefore its clinical use warrants further exploration. Despite the greatly improved resolution compared to IVUS, the penetration depth of OCT is limited in lipid-containing plaque, and therefore, the full thickness of the artery wall may, in some cases, not be visible. As a result, certain measurements that require visualization of the external elastic membrane, such as plaque burden, cannot be reliably performed with OCT. Despite this limitation, it is expected that OCT use will increase and will complement or even replace IVUS for many clinical applications, including thrombus and superficial plaque characterization, evaluating the results of stent placement, lesion coverage, apposition of stent struts to the vessel wall, and edge dissections.

PS-OCT

PS-OCT is an extension to OCT technology that provides a quantitative measure of a property of tissue called birefringence, which alters the polarization of light and is correlated to proteins and macromolecules with oriented structure, such as collagen and actin (97–99). In 2006, a quantitative study examining utility of PS-OCT to measure tissue birefringence of aortic plaques was performed by Nadkarni et al. (37). The study revealed that increased PS-OCT birefringence was correlated to abundant thick collagen fibers and/or the presence of intimal SMC, suggesting that the detection of high birefringence in PS-OCT images may imply increased plaque stability (Fig. 6). Additional ex vivo studies have been reported demonstrating the potential of PS-OCT for the assessment of plaque collagen (100) and for distinguishing between normal intima, fibrous, lipid-rich, and calcific plaques (101). While promising ex vivo imaging results have been reported, the translation of this technology to the clinical setting for evaluating coronary arteries has been slow due to technical challenges, specifically in maintaining the polarization state of the light as it travels through the rapidly rotating catheters. Recently, however, a number of solutions to this dilemma were introduced (102–105), and in 2008, ex vivo results from a catheter-based intracoronary PS-OFDI system with frequency multiplexing were reported (106). If successful, PS-OFDI

may provide additional information regarding the structural integrity of the coronary artery and associated plaques that cannot be inferred from standard OCT images alone. Pilot studies investigating the usefulness of PS-OFDI in patients are currently underway (107), and given that the addition of PS capabilities does not change the standard approach for conducting intracoronary OFDI, it is reasonable to presume that, if clinically useful, PS detection may be a feature incorporated into future commercially available intracoronary OCT systems.

Laser Speckle Imaging

Laser Speckle Imaging (LSI) measures the biomechanical properties of atherosclerotic plaques by evaluating time-varying laser speckle patterns (Fig. 1). When a scattering medium such as tissue is imaged using temporally coherent light from a laser, a granular pattern of multiple bright and dark spots, known as speckle, becomes apparent in the image as a result of the interference of photons returning from different regions within the tissue. In tissue, the Brownian motion of endogenous light scattering particles causes scatter locations and optical path lengths to dynamically change, resulting in time-dependent intensity modulations of the laser speckle. The rate of laser speckle modulation is highly dependent on the motion of endogenous scatterers, which is in turn influenced by the viscoelasticity of the medium (108).

Using these principles, a study conducted on ex vivo arteries has demonstrated that the measurement of the decorrelation time constant of intensity modulations of time-varying laser speckle patterns provides a method for characterizing atherosclerotic plaques and for detecting unstable necrotic core plaques with a sensitivity of 100% and a specificity of 93% (Fig. 7) (38). By combining the analysis of spatial and temporal information from laser speckle patterns, it has been demonstrated that LSI may additionally provide a measure of plaque fibrous cap thickness (109). A recent study has shown that LSI can be conducted through small diameter optical fiber bundles, allowing the opportunity to conduct intracoronary LSI through miniaturized intravascular catheters (110). At present, however, a clinically viable LSI system has yet to be developed and tested, although active research and development in this area is ongoing. If successfully translated into the clinical realm, the intracoronary LSI technique offers the possibility of obtaining a measure of the biomechanical properties of coronary plaques, a feature that is currently not measured with other intravascular optical imaging modalities.

Near-Infrared Spectroscopy

Spectroscopy is the study of the electromagnetic spectrum when light interacts with molecules. Intracoronary diffuse reflectance near-infrared spectroscopy (NIRS) is conducted by evaluating the absorbance of light at different wavelengths in the near-infrared spectrum (1,000 to 2,400 nm), assessed by measuring the amount of light remitted from the vessel wall (Fig. 1). Because NIRS is a diffuse technique and the absorption is accumulated as the light scatters throughout the tissue, the detected absorption spectra necessitate the use of computational algorithms (“chemometrics”) to extract the desired chemical information. In 1993, NIRS was first used to assess the atherosclerotic plaque in the hypercholesterolemic rabbit aorta (111), and after this initial demonstration, a number of groups have reported on the use of NIRS for the assessment of the human arterial wall in ex vivo autopsy studies (Fig. 8) (39,112–114). However, it was not until 2002 that Moreno et al. (114) demonstrated the ability of NIRS to detect many of the typical hallmarks of the unstable plaque including lipid pools (90% sensitivity, 93% specificity), thin fibrous caps (77% sensitivity, 93% specificity), and inflammatory cells (84% sensitivity, 91% specificity). That study provided the necessary support for the continued development of a clinically viable intracoronary

NIRS system. Miniaturized intracoronary catheters for NIR spectroscopy were constructed (115,116), and the first demonstration of intracoronary NIRS in patients was reported in 2006 (117,118).

After these initial pre-clinical– and clinical-proof of principle demonstrations, a more comprehensive validation study of intracoronary NIRS was published in 2009 by Waxman et al. (119) in 106 patients. The goal of the study was to compare the NIRS spectra obtained in vivo to spectra previously obtained and validated by histology in autopsy specimens, which was found to be similar in 83% of cases in which adequate spectra were obtained (95% confidence interval: 70% to 93%). The mean pull-back length over which spectra was obtained was 54.4 ± 22.8 mm, and imaging was performed at a rate of 0.5 mm/s (119). This study demonstrated that NIRS can be safely and successfully performed in living patients for the detection of lipid-containing coronary plaques, through blood and in the presence of cardiac motion. An important advantage of this technique, as it is implemented clinically, is that the NIRS signature can be transmitted through whole blood, and as a result does not require removal of blood from the artery lumen. The LipiScan system (InfraReDx, Burlington, Massachusetts) was recently approved by the FDA for human coronary use. NIRS has additionally been incorporated into a dual functioning catheter that provides simultaneous IVUS and NIRS imaging with an automated longitudinal pullback of 0.5 mm/s, with 360° vessel imaging (120). The introduction of these catheters into the coronary artery can be performed with ease, and imaging may be conducted over long arterial segments including relatively distal segments.

Initial studies have demonstrated the diagnostic potential of this imaging modality (117–119,121), including the identification of lipid pool plaques that may be at higher risk for plaque rupture and the development of acute coronary syndromes. Furthermore, it has been hypothesized that large lipid pool plaques can be associated with increased rates of periprocedural complications, like increased rates of myocardial injury, marker elevations, side-branch obstruction, and distal embolization of the lipid pool that may result in the so-called slow/no-flow phenomenon (121). The COLOR (Chemometric Observations of Lipid Core Plaque of Interest in Native Coronary Arteries) registry is currently evaluating the long-term significance of lipid-core plaques that are detected with the LipiScan system in 1,000 patients. This study will no doubt help to understand the clinical significance of these NIRS-enabled findings. In addition, studies are being conducted to understand the risk of embolization and side-brunch compromise by large lipid-containing plaques. With expanding clinical experience and research, NIRS may play a key future role in improving diagnosis and treatment of patients with coronary artery disease.

Raman Spectroscopy

Raman spectroscopy (400 to 2,000 cm^{-1}) (122,123), including high wavenumber Raman spectroscopy (~2,400 to 3,800 cm^{-1}) (124), is another method that provides a quantitative measure of the chemical composition of biological tissues. When light is incident on tissue, the majority of photons that collide with molecules will scatter with the same frequency and wavelength as the incident photons. A small portion of the incident photons may, however, be scattered with a different frequency as a consequence of an energy exchange between the molecule and colliding photon (Raman scattering) (Fig. 1). This change in energy is equal to the differences of the vibrational and rotational energy levels of the molecule and is unique to specific chemical compounds. Therefore, by measuring and performing comparative analyses of the Raman spectra of the arterial tissue of interest against Raman spectra of known chemical constituents commonly found in arterial tissues, the relative chemical composition of the tissue can be determined.

Raman spectroscopy has been shown to provide a highly specific detection of chemical constituents such as elastin, collagen, cholesterol, cholesterol esters, triglycerides, phospholipids, and calcium salts and has been successfully utilized for the chemical analysis of human atherosclerotic plaques (122,123,125–128) (Fig. 9). Used in conjunction with optical catheters designed with independent illumination and collection fibers (127,129,130), Raman spectroscopy has been demonstrated in vivo for the analysis of the femoral and carotid artery, and the aortic arch in sheep (131), of carotid plaques in patients (128,130), and ex vivo for interrogating coronary artery segments obtained from autopsy samples (127,132). Although first demonstrated in 1992, Raman spectroscopy has not progressed toward a clinically viable intracoronary imaging technology as rapidly as other optical imaging techniques such as OCT. That may be in part due to the very low intensity of the Raman spectra detected from the tissue when implemented in fiber-based imaging catheters. Catheter-based high-wavenumber Raman spectroscopy systems are less affected by the noise generated in the fibers, and as the development of high-wavenumber Raman spectroscopy is relatively new, it remains to be seen when this technology will be introduced clinically.

Fluorescence Spectroscopy

Fluorescence spectroscopy measures the short-lived fluorescence that is emitted from a molecule after excitation by light. In early studies, diagnostic algorithms were developed by measuring differences in tissue fluorescence spectra of collagen, elastin, calcium and lipids, which were demonstrated to broadly discriminated between normal artery and atherosclerotic plaque with a high sensitivity and specificity (133–135). To further increase the specificity for the detection of various constituents in atherosclerotic plaques and for improved plaque characterization, the use of time-resolved laser-induced fluorescence spectroscopy (TR-LIFS) was investigated. TR-LIFS has been demonstrated using pulsed sampling (337 nm, 700 ps pulse width) and gated detection (136,137), resulting in an increased resolution of the spectral overlap of individual chromophores in plaques (138). Studies have demonstrated the successful implementation of TR-LIFS for the ex vivo characterization of atherosclerotic plaque (139). Using this technique, macrophage foams cells were detected with high sensitivity (>85%) and specificity (>95%) in rabbit model in vivo (140), and very recently, a study was reported using TR-LIFS for the evaluation of carotid artery lesions in patients by Marcu et al. (141). This study demonstrated that TR-LIFS can be used to classify tissues into 3 plaque categories including intimal thickening, fibrotic and fibrocalcific plaques, and inflammation and necrotic lesions, and can additionally determine the plaque biochemical content including elastin, collagen, inflammatory cells, and necrosis (141). Recent advancements in fluorescence spectroscopy techniques have enhanced the potential clinical utility of this optical diagnostic modality by increasing the field of view facilitating 2-dimensional mapping of detected fluorophore distributions (142). This new approach, termed fluorescence lifetime imaging microscopy (FLIM), utilizes a gated intensified charge coupled device camera, a pulsed laser source (337 nm, 700 ps pulse width), a fiber bundle/lens configuration for increased field of view, and a filter wheel for selective collection of emission wavelengths (143). Using this system, the authors mapped the fluorescence lifetime of human aorta samples ex vivo and, although preliminary, demonstrated a shift in the measured lifetimes of elastin fluorescence emission in the normal artery and collagen and lipid-rich regions in the atherosclerotic artery (Fig. 10) consistent with prior TR-LIFS studies (143). Fluorescence spectroscopy techniques, specifically TR-LIFS and FLIM, have been demonstrated to provide information on the biochemical composition of arterial tissue and to differentiate between both normal and atherosclerotic tissue regions of interest. Although the results of this technology appear promising, TR-LIFS and FLIM have yet to be incorporated into clinical systems and catheters suitable for human use.

Near-Infrared Fluorescence Molecular Imaging

Optical molecular imaging techniques enable the visualization of molecules that have been labeled with a fluorescent compound (Fig. 1). Recent advances in cardiovascular biology and biochemistry and in optical imaging technologies, in particular intravascular near-infrared fluorescence imaging (NIRF) (40), have increased the potential for molecular imaging of atherosclerosis. Rather than operating in the visible region, NIRF utilizes imaging agents with emission wavelengths of between 650 nm and 1,000 nm. This shift in wavelength offers advantages over conventional fluorescence imaging techniques, including an increase in the penetration depth due to a reduction in the photon absorption from blood hemoglobin, lipid, and water, and a reduction in the detected tissue autofluorescence, leading to a significant increase in the signal-to-noise ratio, or target-to-background ratio of the NIRF imaging agents.

NIRF was recently demonstrated in human carotid plaque specimens using a 1-dimensional fiber-based catheter (144), and was subsequently demonstrated in the iliac vessels of balloon-injured, cholesterol-fed rabbits in vivo (Fig. 11) (145–147). This study was conducted using a protease-activatable NIRF imaging agent (Prosense750, VisEn Medical, Woburn, Massachusetts) used to detect cysteine protease enzyme activity in vivo (148), and therefore, may provide insight to the inflammatory pathways within atherosclerotic lesions. While a number of NIRF imaging agents are currently in development and have been demonstrated to enable visualization of atheroma inflammation, calcification, and angiogenesis (40), the results obtained with the NIRF catheter demonstrate the significant potential for this imaging technology. Although NIRF has great potential for expanding our diagnostic capabilities for coronary arteries, it is still in the early stages of development. In addition to necessary developments in the imaging technology, the future clinical use of NIRF also requires the development and regulatory approval of new-targeted diagnostic imaging agents.

Multimodality Imaging

In many cases, the imaging technologies outlined in this review provide complementary information regarding coronary artery composition and structure to other optical and nonoptical imaging modalities. Therefore, the future of clinical intravascular imaging may lie in multimodality imaging systems that combine 2 or more imaging technologies to more comprehensively assess coronary pathology. The fusion of optical imaging technologies, while still in the early stages of development, is currently the focus of many leading research laboratories with investigators conducting preliminary feasibility and proof-of-principle studies evaluating complementary coregistered imaging technologies and developing prototype hybrid systems and catheters. Examples of multimodality or hybrid systems include OCT and fluorescence spectroscopy (41), combined reflectance, fluorescence, and Raman spectroscopy (42), and OCT and FLIM (149); while optical/nonoptical hybrid devices include OCT and positron detection (150), NIRS and IVUS (151,152), and OCT and IVUS (153,154).

Arguably the most advanced clinical intravascular multimodality optical/nonoptical imaging technology is the NIRS-IVUS system by InfraReDx Inc. that has recently received FDA approval for clinical use (120). Although it is clear that large prospective studies are required to further evaluate the clinical utility of this technology, the first case studies demonstrating the use in patients have recently been published (151,152). The combined NIRS-IVUS imaging system provides physicians with a powerful tool to evaluate the structure of the coronary artery using the IVUS technology, and to provide an index of lipid content by NIRS. Although similar information on coronary pathology may be obtained

using stand-alone IVUS and NIRS imaging systems, the benefits of combining multiple complementary imaging technologies into single multimodal systems and catheters directly translates to an increase in intracoronary information without increasing coronary instrumentation, catheterization times, the risk of complications, and cost. In addition, the registration accuracy between the imaging sets, and therefore the correct interpretation of the coronary pathology, will undoubtedly be increased in the multimodality systems. Given the apparent need for multiple imaging technologies to more comprehensively assess the coronary arteries, we will no doubt see a significant increase in the number of hybrid multimodality imaging systems that may include one or more optical imaging techniques in the near future.

Conclusions

Table 1 summarizes many of the key characteristics of the intravascular imaging modalities discussed in this review, including: 1) the optical mechanism behind the imaging modality; 2) the arterial properties measured; 3) the resolution of the technology; and 4) the current status of the technology in relation to clinical translation and adoption.

Of the imaging modalities described, angioscopy, NIRS, and OCT/OFDI are commercially available and are approved for human use; however, it remains to be determined what impact these imaging modalities will have in clinical practice. LSI, fluorescence spectroscopy, NIRF imaging, Raman spectroscopy, and PS-OCT have yet to make the successful transition to the clinical setting, and many have technical hurdles remaining to be addressed before translation, including solving issues such as the interference of the optical signal from blood in the artery and motion artifacts. For widespread adoption to occur, extensive safety, efficacy, standardization, and validation are required of all imaging techniques. OCT/OFDI has sufficient resolution to enable visualization of the majority of the features associated with the vulnerable plaque; however, it does not provide the same biochemical information available with NIRS or the biomechanical analyses from LSI. Likewise, OCT/OFDI is the only modality that enables quantitative analyses of stent placement, apposition and strut coverage, and could provide significant new insight into mechanisms of stent healing of current and next generation coronary stents. The future of intracoronary optical imaging may, therefore, lie in a combination of these complementary imaging modalities producing a synergistic assessment of the artery wall.

The ideal intracoronary optical imaging technique should be atraumatic, safe, and should facilitate rapid and systematic assessment of the entire coronary arteries, with accurate detection and diagnosis of coronary artery pathology, and should additionally provide sufficient detail to facilitate study of the evolution and etiology of the disease process. Intravascular optical imaging of the coronary arteries may provide a better assessment tool for tailoring and monitoring pharmacological and PCI interventions than the current standard of care methods. Although there are currently no proven therapies for reducing the risk of rupture of the vulnerable plaque, optical imaging techniques may additionally prove useful in further developing our current understanding of this disease process through longitudinal imaging studies.

Acknowledgments

The authors gratefully acknowledge the contributions of Yasunori Ueda, James A. Goldstein, James F. Brennan, and Laura Marcu.

Dr. Suter is supported by National Institutes of Health (NIH) grant R00CA134920. Dr. Nadkarni is supported by NIH grants R21HL088306 and R21HL089203. NIH grants R01HL076398 and R01HL093717 support the cardiovascular imaging research in the laboratory of Drs. Bouma and Tearney; and the Terumo Corporation, Tokyo,

Japan, supports the nonclinical cardiovascular imaging research in the laboratory of Drs. Bouma and Tearney. Dr. Jaffer has received honoraria from Boston Scientific.

ABBREVIATIONS AND ACRONYMS

BMS	bare-metal stent
DES	drug-eluting stent
FD	frequency domain
FDA	Food and Drug Administration
FLIM	fluorescence lifetime imaging microscopy
IVUS	intravascular ultrasonography
LSI	laser speckle imaging
NIRF	near-infrared fluorescence
NIRS	near-infrared spectroscopy
OCT	optical coherence tomography
OFDI	optical frequency domain imaging
PCI	percutaneous coronary intervention
PS	polarization sensitive
SMC	smooth muscle cell
TD	time domain
TR-LIFS	time-resolved laser-induced fluorescence spectroscopy

REFERENCES

1. American Heart Association. Heart Disease and Stroke Statistics—2009 Update. Dallas, Texas: American Heart Association; 2009.
2. Kolodgie FD, Burke AP, Farb A, et al. The thin-cap fibroatheroma: a type of vulnerable plaque: the major precursor lesion to acute coronary syndromes. Curr Opin Cardiol. 2001; 16:285–292. [PubMed: 11584167]
3. Schaar JA, Muller JE, Falk E, et al. Terminology for high-risk and vulnerable coronary artery plaques. Report of a meeting on the vulnerable plaque, June 17 and 18, 2003, Santorini, Greece. Eur Heart J. 2004; 25:1077–1082. [PubMed: 15191780]
4. Virmani R, Kolodgie FD, Burke AP, Farb A, Schwartz SM. Lessons from sudden coronary death: a comprehensive morphological classification scheme for atherosclerotic lesions. Arterioscler Thromb Vasc Biol. 2000; 20:1262–1275. [PubMed: 10807742]
5. Schroeder AP, Falk E. Vulnerable and dangerous coronary plaques. Atherosclerosis. 1995; 118(Suppl):141–149.
6. Bauriedel G, Hutter R, Welsch U, Bach R, Sievert H, Luderitz B. Role of smooth muscle cell death in advanced coronary primary lesions: implications for plaque instability. Cardiovasc Res. 1999; 41:480–488. [PubMed: 10341848]
7. Newby AC, Zaltsman AB. Fibrous cap formation or destruction—the critical importance of vascular smooth muscle cell proliferation, migration and matrix formation. Cardiovasc Res. 1999; 41:345–360. [PubMed: 10341834]
8. Rekhter MD, Hicks GW, Brammer DW, et al. Hypercholesterolemia causes mechanical weakening of rabbit atheroma: local collagen loss as a prerequisite of plaque rupture. Circ Res. 2000; 86:101–108. [PubMed: 10625311]

9. Slager CJ, Wentzel JJ, Gijsen FJ, et al. The role of shear stress in the destabilization of vulnerable plaques and related therapeutic implications. Nat Clin Pract Cardiovasc Med. 2005; 2:456–464. [PubMed: 16265586]
10. Deguchi JO, Aikawa E, Libby P, et al. Matrix metalloproteinase-13/collagenase-3 deletion promotes collagen accumulation and organization in mouse atherosclerotic plaques. Circulation. 2005; 112:2708–2715. [PubMed: 16230484]
11. Richardson PD, Davies MJ, Born GV. Influence of plaque configuration and stress distribution on fissuring of coronary atherosclerotic plaques. Lancet. 1989; 2:941–944. [PubMed: 2571862]
12. Loree HM, Kamm RD, Stringfellow RG, Lee RT. Effects of fibrous cap thickness on peak circumferential stress in model atherosclerotic vessels. Circ Res. 1992; 71:850–858. [PubMed: 1516158]
13. Ohayon J, Teppaz P, Finet G, Rioufol G. In-vivo prediction of human coronary plaque rupture location using intravascular ultrasound and the finite element method. Coron Artery Dis. 2001; 12:655–663. [PubMed: 11811331]
14. Tang D, Yang C, Kobayashi S, Ku DN. Effect of a lipid pool on stress/strain distributions in stenotic arteries: 3-D fluid-structure interactions (FSI) models. J Biomech Eng. 2004; 126:363–370. [PubMed: 15341174]
15. Ohayon J, Finet G, Gharib AM, et al. Necrotic core thickness and positive arterial remodeling index: emergent biomechanical factors for evaluating the risk of plaque rupture. Am J Physiol Heart Circ Physiol. 2008; 295:H717–H727. [PubMed: 18586893]
16. Eskandari H, Salcudean SE, Rohling R, Ohayon J. Viscoelastic characterization of soft tissue from dynamic finite element models. Phys Med Biol. 2008; 53:6569–6590. [PubMed: 18978443]
17. Le Floc'h S, Ohayon J, Tracqui P, et al. Vulnerable atherosclerotic plaque elasticity reconstruction based on a segmentation-driven optimization procedure using strain measurements: theoretical framework. IEEE Trans Med Imaging. 2009; 28:1126–1137. [PubMed: 19164080]
18. Falk E, Shah PK, Fuster V. Coronary plaque disruption. Circulation. 1995; 92:657–671. [PubMed: 7634481]
19. Lee RT, Libby P. The unstable atheroma. Arterioscler Thromb Vasc Biol. 1997; 17:1859–1867. [PubMed: 9351346]
20. Meier P, Zbinden R, Togni M, et al. Coronary collateral function long after drug-eluting stent implantation. J Am Coll Cardiol. 2007; 49:15–20. [PubMed: 17207716]
21. Nebeker JR, Virmani R, Bennett CL, et al. Hypersensitivity cases associated with drug-eluting coronary stents: a review of available cases from the Research on Adverse Drug Events and Reports (RADAR) project. J Am Coll Cardiol. 2006; 47:175–181. [PubMed: 16386683]
22. Togni M, Windecker S, Cocchia R, et al. Sirolimus-eluting stents associated with paradoxic coronary vasoconstriction. J Am Coll Cardiol. 2005; 46:231–236. [PubMed: 16022947]
23. Hassan AK, Bergheanu SC, Stijnen T, et al. Late stent malapposition risk is higher after drug-eluting stent compared with bare-metal stent implantation and associates with late stent thrombosis. Eur Heart J. 2010; 31:1172–1180. [PubMed: 19158118]
24. Sherman CT, Litvack F, Grundfest W, et al. Coronary angioscopy in patients with unstable angina pectoris. N Engl J Med. 1986; 315:913–919. [PubMed: 3489893]
25. Tearney GJ, Jang IK, Bouma BE. Optical coherence tomography for imaging the vulnerable plaque. J Biomed Opt. 2006; 11 021002.
26. Bouma BE, Tearney GJ, Yabushita H, et al. Evaluation of intracoronary stenting by intravascular optical coherence tomography. Heart. 2003; 89:317–320. [PubMed: 12591841]
27. Toutouzas K, Vaina S, Riga MI, Stefanadis C. Evaluation of dissection after coronary stent implantation by intravascular optical coherence tomography. Clin Cardiol. 2009; 32:E47–E48. [PubMed: 17803241]
28. Regar E, Schaar J, Serruys PW. Images in cardiology. Acute recoil in sirolimus eluting stent: real time, in vivo assessment with optical coherence tomography. Heart. 2006; 92:123. [PubMed: 16365366]
29. Raffel OC, Hannan JC, Jang IK. Coronary stent malapposition as a result of a post-stenotic aneurysm detected by optical coherence tomography. J Invasive Cardiol. 2006; 18:561–562. [PubMed: 17090823]

30. Sawada T, Shite J, Shinke T, et al. Persistent malapposition after implantation of sirolimus-eluting stent into intramural coronary hematoma: optical coherence tomography observations. Circ J. 2006; 70:1515–1519. [PubMed: 17062980]
31. Takano M, Jang IK, Mizuno K. Neointimal proliferation around malapposed struts of a sirolimus-eluting stent: optical coherence tomography findings. Eur Heart J. 2006; 27:1763. [PubMed: 16476695]
32. Regar E, van Beusekom HM, van der Giessen WJ, Serruys PW. Images in cardiovascular medicine. Optical coherence tomography findings at 5-year follow-up after coronary stent implantation. Circulation. 2005; 112:e345–e346. [PubMed: 16330689]
33. Barlis P, Tanigawa J, Di Mario C. Coronary bioabsorbable magnesium stent: 15-month intravascular ultrasound and optical coherence tomography findings. Eur Heart J. 2007; 28:2319. [PubMed: 17485484]
34. Gupta R, Raffel OC, Jang IK. Severe intimal hyperplasia after sirolimus eluting stent deployment: evaluation by optical coherence tomography. Heart. 2007; 93:754. [PubMed: 17502657]
35. Tanigawa J, Barlis P, Di Mario C. Do unapposed stent struts endothelialise? In vivo demonstration with optical coherence tomography. Heart. 2007; 93:378. [PubMed: 17322520]
36. Takano M, Inami S, Jang IK, et al. Evaluation by optical coherence tomography of neointimal coverage of sirolimus-eluting stent three months after implantation. Am J Cardiol. 2007; 99:1033–1038. [PubMed: 17437723]
37. Nadkarni SK, Pierce MC, Park BH, et al. Measurement of collagen and smooth muscle cell content in atherosclerotic plaques using polarization-sensitive optical coherence tomography. J Am Coll Cardiol. 2007; 49:1474–1481. [PubMed: 17397678]
38. Nadkarni SK, Bouma BE, Helg T, et al. Characterization of atherosclerotic plaques by laser speckle imaging. Circulation. 2005; 112:885–892. [PubMed: 16061738]
39. Wang J, Geng YJ, Guo B, et al. Near-infrared spectroscopic characterization of human advanced atherosclerotic plaques. J Am Coll Cardiol. 2002; 39:1305–1313. [PubMed: 11955848]
40. Jaffer FA, Libby P, Weissleder R. Optical and multimodality molecular imaging: insights into atherosclerosis. Arterioscler Thromb Vasc Biol. 2009; 29:1017–1024. [PubMed: 19359659]
41. Barton JK, Guzman F, Tumlinson A. Dual modality instrument for simultaneous optical coherence tomography imaging and fluorescence spectroscopy. J Biomed Optics. 2004; 9:618–623.
42. Scepanovic OR, Volynskaya Z, Kong CR, Galindo LH, Dasari RR, Feld MS. A multimodal spectroscopy system for real-time disease diagnosis. Rev Sci Instrum. 2009; 80 043103.
43. Barlis P, Schmitt JM. Current and future developments in intracoronary optical coherence tomography imaging. EuroIntervention. 2009; 4:529–533. [PubMed: 19284077]
44. Bhatia V, Bhatia R, Dhindsa S, Dhindsa M. Imaging of the vulnerable plaque: new modalities. South Med J. 2003; 96:1142–1147. [PubMed: 14632365]
45. Glaudemans AW, Slart RH, Bozzao A, et al. Molecular imaging in atherosclerosis. Eur J Nucl Med Mol Imaging. 2010; 37:2381–2397. [PubMed: 20306036]
46. Koh AS, Chia S. Update on clinical imaging of coronary plaque in acute coronary syndrome. Ann Acad Med Singapore. 2010; 39:203–209. [PubMed: 20372756]
47. Prati F, Regar E, Mintz GS, et al. Expert review document on methodology, terminology, and clinical applications of optical coherence tomography: physical principles, methodology of image acquisition, and clinical application for assessment of coronary arteries and atherosclerosis. Eur Heart J. 2010; 31:401–415. [PubMed: 19892716]
48. Choi SH, Chae A, Chen CH, Merki E, Shaw PX, Tsimikas S. Emerging approaches for imaging vulnerable plaques in patients. Curr Opin Biotechnol. 2007; 18:73–82. [PubMed: 17234398]
49. Hamdan A, Assali A, Fuchs S, Battler A, Kornowski R. Imaging of vulnerable coronary artery plaques. Catheter Cardiovasc Interv. 2007; 70:65–74. [PubMed: 17585387]
50. Maehara A, Mintz GS, Weissman NJ. Advances in intravascular imaging. Circ Cardiovasc Interv. 2009; 2:482–490. [PubMed: 20031760]
51. Sharif F, Murphy RT. Current status of vulnerable plaque detection. Catheter Cardiovasc Interv. 2010; 75:135–144. [PubMed: 19670307]

52. Garcia-Garcia HM, Gonzalo N, Granada JF, Regar E, Serruys PW. Diagnosis and treatment of coronary vulnerable plaques. Expert Rev Cardiovasc Ther. 2008; 6:209–222. [PubMed: 18248275]
53. Mizuno K, Miyamoto A, Satomura K, et al. Angioscopic coronary macromorphology in patients with acute coronary disorders. Lancet. 1991; 337:809–812. [PubMed: 1672912]
54. Kubo T, Imanishi T, Takarada S, et al. Implication of plaque color classification for assessing plaque vulnerability: a coronary angioscopy and optical coherence tomography investigation. J Am Coll Cardiol Intv. 2008; 1:74–80.
55. Uchida Y, Nakamura F, Tomaru T, et al. Prediction of acute coronary syndromes by percutaneous coronary angioscopy in patients with stable angina. Am Heart J. 1995; 130:195–203. [PubMed: 7631596]
56. Ueda Y, Ohtani T, Shimizu M, Hirayama A, Kodama K. Assessment of plaque vulnerability by angioscopic classification of plaque color. Am Heart J. 2004; 148:333–335. [PubMed: 15309005]
57. Tawakol A, Muller J. Through the looking glass: an angioscopic view of the effect of statin therapy on coronary artery plaques. J Am Coll Cardiol. 2003; 42:687–689. [PubMed: 12932602]
58. Takano M, Mizuno K, Yokoyama S, et al. Changes in coronary plaque color and morphology by lipid-lowering therapy with atorvastatin: serial evaluation by coronary angioscopy. J Am Coll Cardiol. 2003; 42:680–686. [PubMed: 12932601]
59. Yokoyama S, Takano M, Yamamoto M, et al. Extended follow-up by serial angioscopic observation for bare-metal stents in native coronary arteries: from healing response to atherosclerotic transformation of neointima. Circ Cardiovasc Interv. 2009; 2:205–212. [PubMed: 20031717]
60. Yamamoto M, Okamatsu K, Inami S, et al. Relationship between neointimal coverage of sirolimus-eluting stents and lesion characteristics: a study with serial coronary angioscopy. Am Heart J. 2009; 158:99–104. [PubMed: 19540398]
61. Ishibashi F, Yokoyama S, Miyahara K, et al. Quantitative colorimetry of atherosclerotic plaque using the L*a*b* color space during angioscopy for the detection of lipid cores underneath thin fibrous caps. Int J Cardiovasc Imaging. 2007; 23:679–691. [PubMed: 17318361]
62. Huang D, Swanson EA, Lin CP, et al. Optical coherence tomography. Science. 1991; 254:1178–1181. [PubMed: 1957169]
63. Tearney GJ, Brezinski ME, Bouma BE, et al. In vivo endoscopic optical biopsy with optical coherence tomography. Science. 1997; 276:2037–2039. [PubMed: 9197265]
64. Leitgeb R, Hitzenberger C, Fercher A. Performance of Fourier domain vs. time domain optical coherence tomography. Opt Express. 2003; 11:889–894. [PubMed: 19461802]
65. Choma M, Sarunic M, Yang C, Izatt J. Sensitivity advantage of swept source and Fourier domain optical coherence tomography. Opt Express. 2003; 11:2183–2189. [PubMed: 19466106]
66. Yun S, Tearney G, de Boer J, Iftimia N, Bouma B. High-speed optical frequency-domain imaging. Opt Express. 2003; 11:2953–2963. [PubMed: 19471415]
67. Yun SH, Tearney GJ, Vakoc BJ, et al. Comprehensive volumetric optical microscopy in vivo. Nature Med. 2006; 12:1429–1433. [PubMed: 17115049]
68. Kume T, Akasaka T, Kawamoto T, et al. Assessment of coronary arterial plaque by optical coherence tomography. Am J Cardiol. 2006; 97:1172–1175. [PubMed: 16616021]
69. MacNeill BD, Jang IK, Bouma BE, et al. Focal and multi-focal plaque macrophage distributions in patients with acute and stable presentations of coronary artery disease. J Am Coll Cardiol. 2004; 44:972–979. [PubMed: 15337206]
70. Rieber J, Meissner O, Babaryka G, et al. Diagnostic accuracy of optical coherence tomography and intravascular ultrasound for the detection and characterization of atherosclerotic plaque composition in ex-vivo coronary specimens: a comparison with histology. Coron Artery Dis. 2006; 17:425–430. [PubMed: 16845250]
71. Tearney GJ, Jang IK, Bouma BE. Evidence of cholesterol crystals in atherosclerotic plaque by optical coherence tomographic (OCT) imaging. Eur Heart J. 2003; 24:1462. [PubMed: 12909076]
72. Tearney GJ, Yabushita H, Houser SL, et al. Quantification of macrophage content in atherosclerotic plaques by optical coherence tomography. Circulation. 2003; 107:113–119. [PubMed: 12515752]

73. Yabushita H, Bouma BE, Houser SL, et al. Characterization of human atherosclerosis by optical coherence tomography. Circulation. 2002; 106:1640–1645. [PubMed: 12270856]
74. Jang IK, Bouma BE, Kang DH, et al. Visualization of coronary atherosclerotic plaques in patients using optical coherence tomography: comparison with intravascular ultrasound. J Am Coll Cardiol. 2002; 39:604–609. [PubMed: 11849858]
75. Kume T, Akasaka T, Kawamoto T, et al. Assessment of coronary arterial thrombus by optical coherence tomography. Am J Cardiol. 2006; 97:1713–1717. [PubMed: 16765119]
76. Kume T, Okura H, Kawamoto T, et al. Relationship between coronary remodeling and plaque characterization in patients without clinical evidence of coronary artery disease. Atherosclerosis. 2008; 197:799–805. [PubMed: 17822707]
77. Tearney GJ, Jang IK, Kang DH, et al. Porcine coronary imaging in vivo by optical coherence tomography. Acta Cardiol. 2000; 55:233–237. [PubMed: 11041121]
78. Jang IK, Tearney G, Bouma B. Visualization of tissue prolapse between coronary stent struts by optical coherence tomography: comparison with intravascular ultrasound. Circulation. 2001; 104:2754. [PubMed: 11723031]
79. Grube E, Gerckens U, Buellesfeld L, Fitzgerald PJ. Images in cardiovascular medicine. Intracoronary imaging with optical coherence tomography: a new high-resolution technology providing striking visualization in the coronary artery. Circulation. 2002; 106:2409–2410. [PubMed: 12403675]
80. Barlis P, Serruys PW, Gonzalo N, van der Giessen WJ, de Jaegere PJ, Regar E. Assessment of culprit and remote coronary narrowings using optical coherence tomography with long-term outcomes. Am J Cardiol. 2008; 102:391–395. [PubMed: 18678293]
81. Jang IK, Tearney GJ, MacNeill B, et al. In vivo characterization of coronary atherosclerotic plaque by use of optical coherence tomography. Circulation. 2005; 111:1551–1555. [PubMed: 15781733]
82. Chia S, Christopher Raffel O, Takano M, Tearney GJ, Bouma BE, Jang IK. In-vivo comparison of coronary plaque characteristics using optical coherence tomography in women vs. men with acute coronary syndrome. Coron Artery Dis. 2007; 18:423–427. [PubMed: 17700211]
83. Kubo T, Imanishi T, Takarada S, et al. Assessment of culprit lesion morphology in acute myocardial infarction: ability of optical coherence tomography compared with intravascular ultrasound and coronary angioscopy. J Am Coll Cardiol. 2007; 50:933–939. [PubMed: 17765119]
84. Raffel OC, Tearney GJ, Gauthier DD, Halpern EF, Bouma BE, Jang IK. Relationship between a systemic inflammatory marker, plaque inflammation, and plaque characteristics determined by intravascular optical coherence tomography. Arterioscler Thromb Vasc Biol. 2007; 27:1820–1827. [PubMed: 17541021]
85. Matsumoto D, Shite J, Shinke T, et al. Neointimal coverage of sirolimuseluting stents at 6-month follow-up: evaluated by optical coherence tomography. Eur Heart J. 2007; 28:961–967. [PubMed: 17135281]
86. Camenzind E, Steg PG, Wijns W. Stent thrombosis late after implantation of first-generation drug-eluting stents: a cause for concern. Circulation. 2007; 115:1440–1455. discussion 1455. [PubMed: 17344324]
87. Garcia-Garcia HM, Gonzalo N, Regar E, Serruys PW. Virtual histology and optical coherence tomography: from research to broad clinical application. Heart. 2009; 95:1362–1374. [PubMed: 19638515]
88. Gonzalo N, Serruys PW, Okamura T, et al. Optical coherence tomography patterns of stent restenosis. Am Heart J. 2009; 158:284–293. [PubMed: 19619707]
89. de Boer JF, Cense B, Park BH, Pierce MC, Tearney GJ, Bouma BE. Improved signal-to-noise ratio in spectral-domain compared with time-domain optical coherence tomography. Opt Lett. 2003; 28:2067–2069. [PubMed: 14587817]
90. Tearney GJ, Waxman S, Shishkov M, et al. Three-dimensional coronary artery microscopy by intracoronary optical frequency domain imaging. J Am Coll Cardiol Img. 2008; 1:752–761.
91. Templin C, Meyer M, Muller MF, et al. Coronary optical frequency domain imaging (OFDI) for in vivo evaluation of stent healing: comparison with light and electron microscopy. Eur Heart J. 2010; 31:1792–1801. [PubMed: 20525979]

92. Takarada S, Imanishi T, Liu Y, et al. Advantage of next-generation frequency-domain optical coherence tomography compared with conventional time-domain system in the assessment of coronary lesion. Catheter Cardiovasc Interv. 2010; 75:202–206. [PubMed: 19937788]

93. Okamura T, Gonzalo N, Gutierrez-Chico JL, et al. Reproducibility of coronary Fourier domain optical coherence tomography: quantitative analysis of in vivo stented coronary arteries using three different software packages. EuroIntervention. 2010; 6:371–379. [PubMed: 20884417]

94. Okamura T, Serruys PW, Regar E. Three-dimensional visualization of intracoronary thrombus during stent implantation using the second generation, Fourier domain optical coherence tomography. Eur Heart J. 2010; 31:625. [PubMed: 19965860]

95. Gonzalo N, Tearney GJ, Serruys PW, et al. Second-generation optical coherence tomography in clinical practice. High-speed data acquisition is highly reproducible in patients undergoing percutaneous coronary intervention. Rev Esp Cardiol. 2010; 63:893–903. [PubMed: 20738934]

96. Imola F, Mallus MT, Ramazzotti V, et al. Safety and feasibility of frequency domain optical coherence tomography to guide decision making in percutaneous coronary intervention. EuroIntervention. 2010; 6:575–581. [PubMed: 21044910]

97. de Boer JF, Milner TE, van Gemert MJC, Nelson JS. Two-dimensional birefringence imaging in biological tissue by polarization-sensitive optical coherence tomography. Optics Lett. 1997; 22:934–936.

98. Everett MJ, Schoenenberger K, Colston BW, da Silva LB. Birefringence characterization of biological tissue by use of optical coherence tomography. Optics Lett. 1998; 23:228–230.

99. de Boer JF, Milner TE. Review of polarization sensitive optical coherence tomography and Stokes vector determination. J Biomed Opt. 2002; 7:359–371. [PubMed: 12175285]

100. Giattina SD, Courtney BK, Herz PR, et al. Assessment of coronary plaque collagen with polarization sensitive optical coherence tomography (PS-OCT). Int J Cardiol. 2006; 107:400–409. [PubMed: 16434114]

101. Kuo WC, Chou NK, Chou C, et al. Polarization-sensitive optical coherence tomography for imaging human atherosclerosis. Appl Opt. 2007; 46:2520–2527. [PubMed: 17429466]

102. Park BH, Pierce MC, Cense B, et al. Real-time fiber-based multifunctional spectral-domain optical coherence tomography at 1.3 um. Optics Express. 2005; 13:3931–3944. [PubMed: 19495302]

103. Park BH, Saxer C, Srinivas SM, Nelson JS, de Boer JF. In vivo burn depth determination by high-speed fiber-based polarization sensitive optical coherence tomography. J Biomed Opt. 2001; 6:474–479. [PubMed: 11728208]

104. Saxer CE, de Boer JF, Park BH, Zhao Y, Chen Z, Nelson JS. High-speed fiber-based polarization-sensitive optical coherence tomography of in vivo human skin. Opt Lett. 2000; 25:1355–1357. [PubMed: 18066215]

105. Zhang J, Jung W, Nelson JS, Chen Z. Full range polarization-sensitive Fourier domain optical coherence tomography. Optics Express. 2004; 12:6033–6039. [PubMed: 19488244]

106. Oh WY, Yun SH, Vakoc BJ, et al. High-speed polarization sensitive optical frequency domain imaging with frequency multiplexing. Optics Express. 2008; 16:1096–1103. [PubMed: 18542183]

107. Suter MJ, Tearney GJ, Oh WY, Bouma BE. Progress in intracoronary optical coherence tomography. IEEE J Select Topics Quantum Electronics. 2010; 16:706–711.

108. Mason TG, Weitz DA. Optical measurements of frequency-dependent linear viscoelasticity moduli of complex fluids. Physical Rev Lett. 1995; 74:1250–1253.

109. Nadkarni SK, Bilenca A, Bouma BE, Tearney GJ. Measurement of fibrous cap thickness in atherosclerotic plaques by spatiotemporal analysis of laser speckle images. J Biomed Opt. 2006; 11 021006.

110. Nadkarni SK, Bouma BE, Yelin D, Gulati A, Tearney GJ. Laser speckle imaging of atherosclerotic plaques through optical fiber bundles. J Biomed Opt. 2008; 13 054016.

111. Cassis LA, Lodder RA. Near-IR imaging of atheromas in living arterial tissue. Anal Chem. 1993; 65:1247–1256. [PubMed: 8503505]

112. Jaross W, Neumeister V, Lattke P, Schuh D. Determination of cholesterol in atherosclerotic plaques using near infrared diffuse reflection spectroscopy. Atherosclerosis. 1999; 147:327–337. [PubMed: 10559519]
113. Neumeister V, Scheibe M, Lattke P, Jaross W. Determination of the cholesterol-collagen ratio of arterial atherosclerotic plaques using near infrared spectroscopy as a possible measure of plaque stability. Atherosclerosis. 2002; 165:251–257. [PubMed: 12417275]
114. Moreno PR, Lodder RA, Purushothaman KR, Charash WE, O'Connor WN, Muller JE. Detection of lipid pool, thin fibrous cap, and inflammatory cells in human aortic atherosclerotic plaques by near-infrared spectroscopy. Circulation. 2002; 105:923–927. [PubMed: 11864919]
115. Zuluaga AF, DeJesus ST. Miniaturized probes for intracoronary optical spectroscopy through blood. Am J Cardiol. 2002; 90:128H–129H. [PubMed: 12106841]
116. Waxman S, Tang J, Marshik BJ, et al. In vivo detection of a coronary artificial target with a near infrared spectroscopy catheter. Am J Cardiol. 2004; 94:141E. [PubMed: 15219529]
117. Caplan JD, Waxman S, Nesto RW, Muller JE. Near-infrared spectroscopy for the detection of vulnerable coronary artery plaques. J Am Coll Cardiol. 2006; 47:C92–C96. [PubMed: 16631516]
118. Waxman S, Ishibashi F, Muller JE. Detection and treatment of vulnerable plaques and vulnerable patients: novel approaches to prevention of coronary events. Circulation. 2006; 114:2390–2411. [PubMed: 17130356]
119. Waxman S, Dixon SR, L'Allier P, et al. In vivo validation of a catheter-based near-infrared spectroscopy system for detection of lipid core coronary plaques: initial results of the SPECTACL study. J Am Coll Cardiol Img. 2009; 2:858–868.
120. Wentzel JJ, van der Giessen AG, Garg S, et al. In vivo 3D distribution of lipid-core plaque in human coronary artery as assessed by fusion of near infrared spectroscopy-intravascular ultrasound and multislice computed tomography scan. Circ Cardiovasc Imaging. 2010; 3:e6–e7. [PubMed: 21081741]
121. Goldstein JA, Grines C, Fischell T, et al. Coronary embolization following balloon dilation of lipid-core plaques. J Am Coll Cardiol Img. 2009; 2:1420–1424.
122. Baraga JJ, Feld MS, Rava RP. In situ optical histochemistry of human artery using near infrared Fourier transform Raman spectroscopy. Proc Natl Acad Sci USA. 1992; 89:3473–3477. [PubMed: 1565640]
123. Manoharan R, Baraga JJ, Feld MS, Rava RP. Quantitative histochemical analysis of human artery using Raman spectroscopy. J Photochem Photobiol B. 1992; 16:211–233. [PubMed: 1474427]
124. Koljenovic S, Bakker Schut TC, Wolthuis R, et al. Tissue characterization using high wave number Raman spectroscopy. J Biomed Opt. 2005; 10 031116.
125. Brennan JF III, Romer TJ, Lees RS, Tercyak AM, Kramer JR Jr, Feld MS. Determination of human coronary artery composition by Raman spectroscopy. Circulation. 1997; 96:99–105. [PubMed: 9236423]
126. Romer TJ, Brennan JF III, Fitzmaurice M, et al. Histopathology of human coronary atherosclerosis by quantifying its chemical composition with Raman spectroscopy. Circulation. 1998; 97:878–885. [PubMed: 9521336]
127. van de Poll SW, Kastelijn K, Bakker Schut TC, et al. On-line detection of cholesterol and calcification by catheter based Raman spectroscopy in human atherosclerotic plaque ex vivo. Heart. 2003; 89:1078–1082. [PubMed: 12923035]
128. Brennan JF III, Nazemi J, Motz J, Ramcharitar S. The vPredict optical catheter system: intravascular Raman spectroscopy. EuroIntervention. 2008; 3:635–638. [PubMed: 19608493]
129. Chau AH, Motz JT, Gardecki JA, Waxman S, Bouma BE, Tearney GJ. Fingerprint and high-wavenumber Raman spectroscopy in a human-swine coronary xenograft in vivo. J Biomed Opt. 2008; 13 040501.
130. Motz JT, Fitzmaurice M, Miller A, et al. In vivo Raman spectral pathology of human atherosclerosis and vulnerable plaque. J Biomed Opt. 2006; 11 021003.
131. Buschman HP, Marple ET, Wach ML, et al. In vivo determination of the molecular composition of artery wall by intravascular Raman spectroscopy. Anal Chem. 2000; 72:3771–3775. [PubMed: 10959962]

132. Nazemi JH, Brennan JF. Lipid concentrations in human coronary artery determined with high wavenumber Raman shifted light. J Biomed Opt. 2009; 14 034009.
133. Richards-Kortum R, Rava RP, Fitzmaurice M, et al. A one-layer model of laser-induced fluorescence for diagnosis of disease in human tissue: applications to atherosclerosis. IEEE Trans Biomed Eng. 1989; 36:1222–1232. [PubMed: 2606498]
134. Baraga JJ, Rava RP, Taroni P, Kittrell C, Fitzmaurice M, Feld MS. Laser induced fluorescence spectroscopy of normal and atherosclerotic human aorta using 306–310 nm excitation. Lasers Surg Med. 1990; 10:245–261. [PubMed: 2345474]
135. Deckelbaum LI, Lam JK, Cabin HS, Clubb KS, Long MB. Discrimination of normal and atherosclerotic aorta by laser-induced fluorescence. Lasers Surg Med. 1987; 7:330–335. [PubMed: 3683063]
136. Fang Q, Papaioannou T, Jo JA, Vaitha R, Shastry K, Marcu L. Time-domain laser-induced fluorescence spectroscopy apparatus for clinical diagnostics. Rev Sci Instrum. 2004; 75:151–162.
137. Sun Y, Liu R, Elson DS, et al. Simultaneous time- and wavelength-resolved fluorescence spectroscopy for near real-time tissue diagnosis. Opt Lett. 2008; 33:630–632. [PubMed: 18347733]
138. Maarek JM, Marcu L, Fishbein MC, Grundfest WS. Time-resolved fluorescence of human aortic wall: use for improved identification of atherosclerotic lesions. Lasers Surg Med. 2000; 27:241–254. [PubMed: 11013386]
139. Marcu L, Fishbein MC, Maarek JM, Grundfest WS. Discrimination of human coronary artery atherosclerotic lipid-rich lesions by time-resolved laser-induced fluorescence spectroscopy. Arterioscler Thromb Vasc Biol. 2001; 21:1244–1250. [PubMed: 11451759]
140. Marcu L, Fang Q, Jo JA, et al. In vivo detection of macrophages in a rabbit atherosclerotic model by time-resolved laser-induced fluorescence spectroscopy. Atherosclerosis. 2005; 181:295–303. [PubMed: 16039283]
141. Marcu L, Jo JA, Fang Q, et al. Detection of rupture-prone atherosclerotic plaques by time-resolved laser-induced fluorescence spectroscopy. Atherosclerosis. 2009; 204:156–164. [PubMed: 18926540]
142. Marcu L. Fluorescence lifetime in cardiovascular diagnostics. J Biomed Opt. 2010; 15 011106.
143. Elson DS, Jo JA, Marcu L. Miniaturized side-viewing imaging probe for fluorescence lifetime imaging (FLIM): validation with fluorescence dyes, tissue structural proteins and tissue specimens. New J Phys. 2007; 9:127.
144. Zhu B, Jaffer FA, Ntziachristos V, Weissleder R. Development of a near infrared fluorescence catheter: operating characteristics and feasibility for atherosclerotic plaque detection. J Physics D Applied Physics. 2005; 38:2701–2707.
145. Jaffer FA, Libby P, Weissleder R. Molecular imaging of cardiovascular disease. Circulation. 2007; 116:1052–1061. [PubMed: 17724271]
146. Jaffer FA, Nahrendorf M, Vinegoni C, et al. In vivo imaging of protease activity in atherosclerosis using a near-infrared fluorescence intravascular catheter. Circulation. 2006; 114:II410.
147. Jaffer FA, Vinegoni C, John MC, et al. Real-time catheter molecular sensing of inflammation in proteolytically active atherosclerosis. Circulation. 2008; 118:1802–1809. [PubMed: 18852366]
148. Weissleder R, Tung CH, Mahmood U, Bogdanov A Jr. In vivo imaging of tumors with protease-activated near-infrared fluorescent probes. Nat Biotechnol. 1999; 17:375–378. [PubMed: 10207887]
149. Park J, Jo JA, Shrestha S, Pande P, Wan Q, Applegate BE. A dual-modality optical coherence tomography and fluorescence lifetime imaging microscopy system for simultaneous morphological and biochemical tissue characterization. Biomed Optics Express. 2010; 1:186–200.
150. Piao D, Sadeghi MM, Zhang J, Chen Y, Sinusas AJ, Zhu Q. Hybrid positron detection and optical coherence tomography system: design, calibration, and experimental validation with rabbit atherosclerotic models. J Biomed Opt. 2005; 10:44010. [PubMed: 16178644]

151. Garg S, Serruys PW, van der Ent M, et al. First use in patients of a combined near infra-red spectroscopy and intra-vascular ultrasound catheter to identify composition and structure of coronary plaque. EuroIntervention. 2010; 5:755–756. [PubMed: 20142232]

152. Schultz CJ, Serruys PW, van der Ent M, et al. First-in-man clinical use of combined near-infrared spectroscopy and intravascular ultrasound: a potential key to predict distal embolization and no-reflow? J Am Coll Cardiol. 2010; 56:314. [PubMed: 20633824]

153. Li X, Yin J, Hu C, Zhou Q, Shung KK, Chen Z. High-resolution coregistered intravascular imaging with integrated ultrasound and optical coherence tomography probe. Appl Phys Lett. 2010; 97 133702.

154. Yin J, Yang HC, Li X, et al. Integrated intravascular optical coherence tomography ultrasound imaging system. J Biomed Opt. 2010; 15 010512.

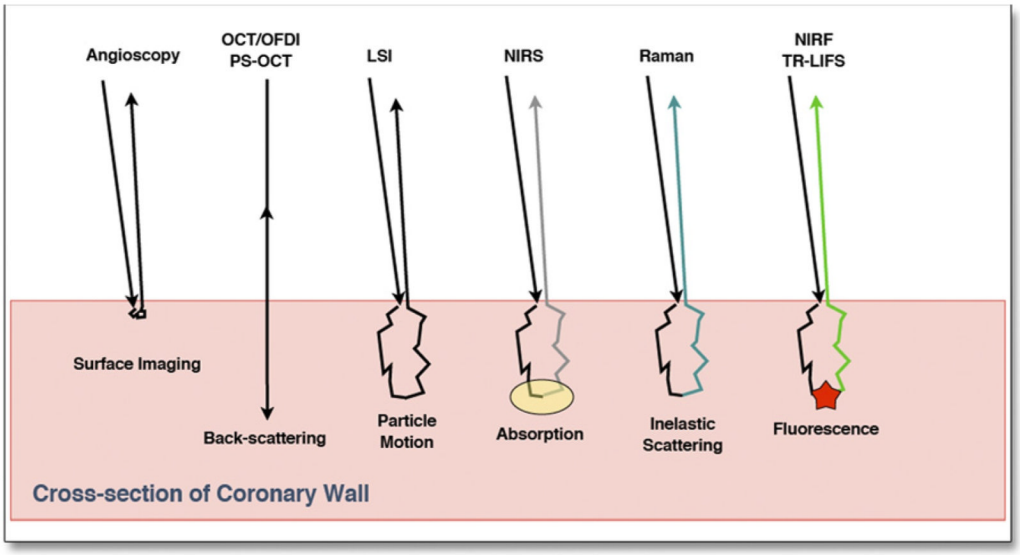

Figure 1. Schematic Diagram

The diagram shows the predominant light/tissue interactions that are detected in each of the intravascular optical imaging modalities discussed in this review. LSI = laser speckle imaging; NIRF = near-infrared fluorescence; NIRS = near-infrared spectroscopy; OCT = optical coherence tomography; OFDI = optical frequency domain imaging; PS = polarization sensitive; TR-LIFS = time-resolved laser-induced fluorescence spectroscopy.

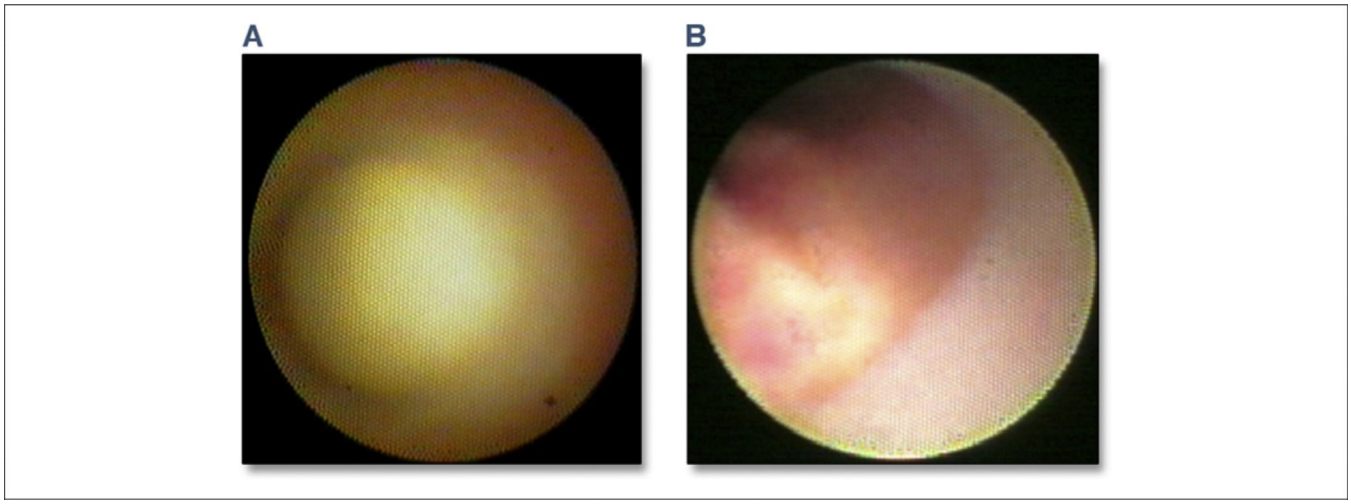

Figure 2. Angioscopy Images Obtained From a Patient In Vivo

(A) An example of a nondisrupted glistening yellow plaque with no evidence of red or white thrombus on the plaque surface. **(B)** A yellow plaque after rupture and subsequent clot formation: mixed thrombus of white and red color is observed on the surface, which has cotton like or ragged appearance and presents fragmentation. Yellow material detected in the thrombus has an irregular surface and is protruding into lumen, which may be the mixture of thrombus and lipid content from the necrotic core. This is a typical angioscopic image of an acute coronary syndrome culprit lesion. Figure courtesy of Yasunori Ueda.

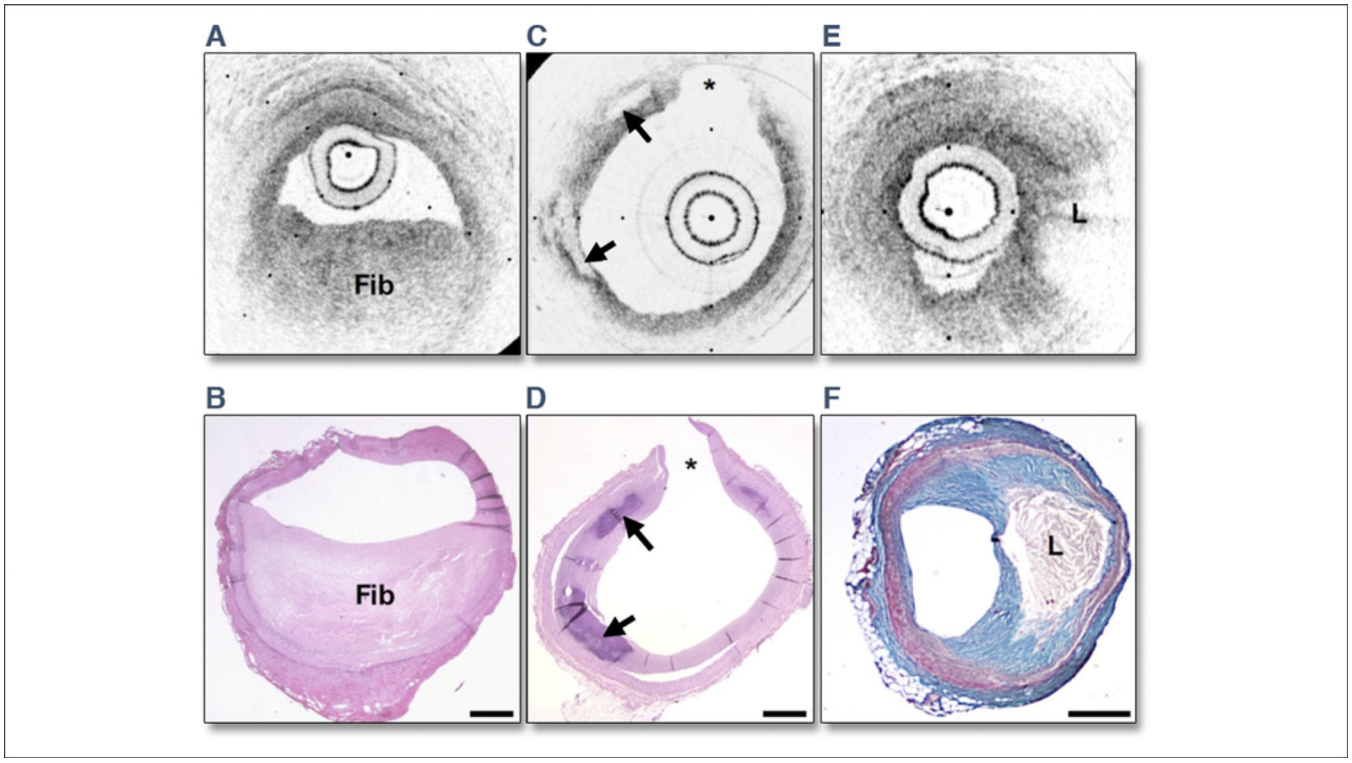

Figure 3. OCT Images and Corresponding Histology

Optical coherence tomography (OCT) images and corresponding histology for **(A, B)** fibrous plaque type, **(C, D)** calcific plaque type, and **(E, F)** lipid-rich plaque type. In fibrous plaques **(A, B)**, the optical coherence tomography (OCT) signal (Fib) is observed to be strong and homogenous. In comparison, both calcific regions **(arrows) (C, D)** and lipid-rich regions (L) **(E, F)** appear as signal-poor regions within the vessel wall. Lipid-rich plaques have diffuse or poorly demarcated borders whereas the borders of calcific nodules are sharply delineated. (**B**, **D**, hematoxylin and eosin; **F**, Masson's trichrome; original magnification ×40.) Scale bars, tick marks = 500 μm. *****Indicates a side branch. Reprinted with permission from Tearney et al. (25).

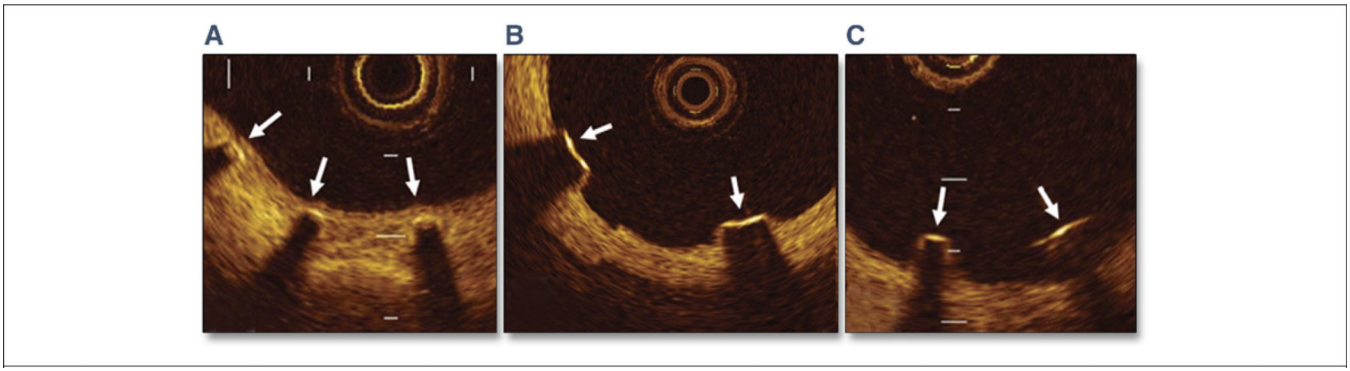

Figure 4. Classification of Sirolimus-Eluting Stent Strut Conditions by OCT

(A) Well-apposed with neointimal coverage **(arrows)**. **(B)** Well-apposed without neointimal coverage **(arrows)**. **(C)** Malapposed without neointimal coverage **(arrows)**. OCT = optical coherence tomography. Reprinted with permission from Matsumoto et al. (85).

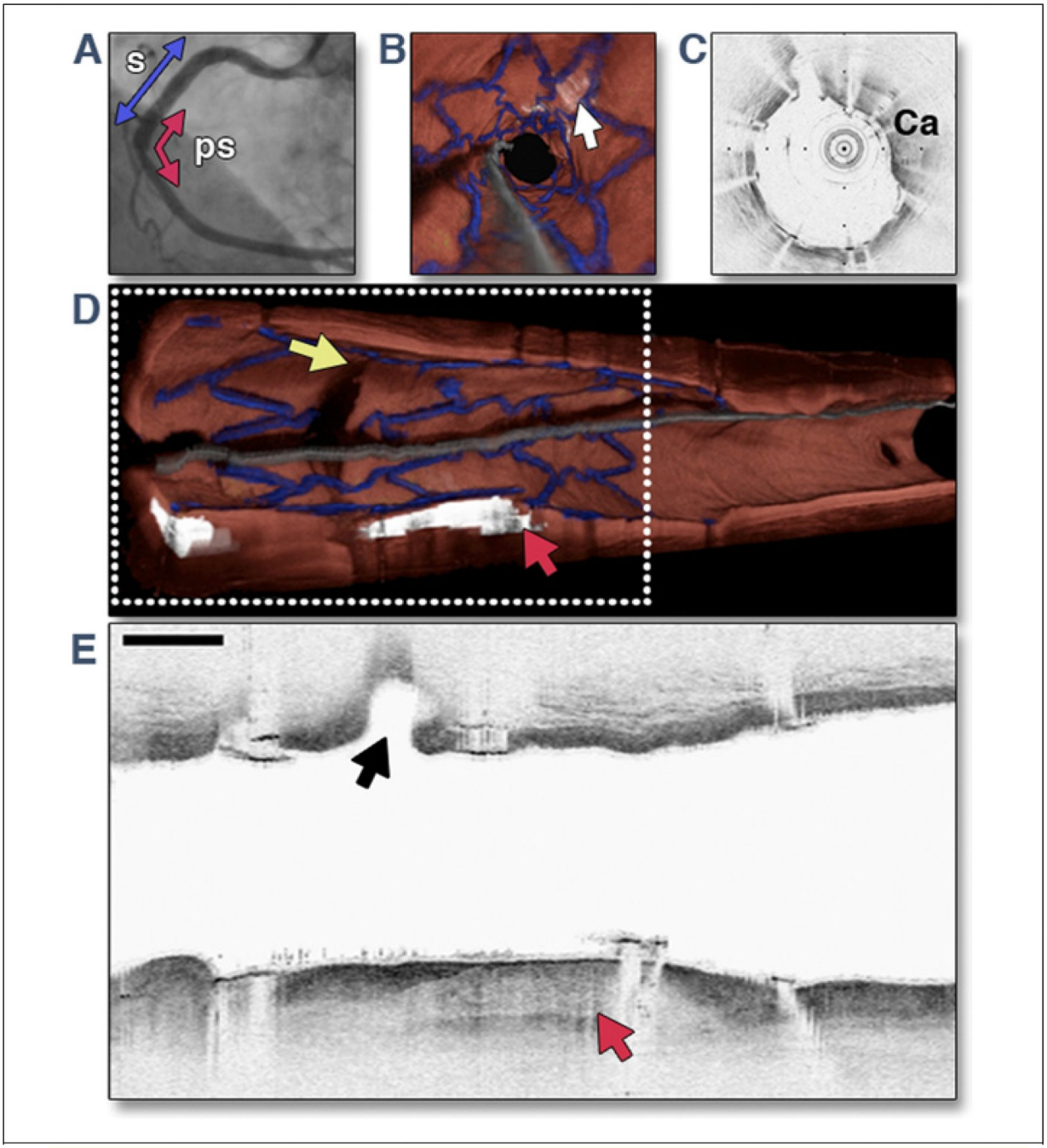

Figure 5. OFDI Images Obtained From Right Coronary Artery of a Patient Immediately After Deployment of DES

The 3.0 cm optical frequency domain imaging (OFDI) pullback was obtained during a lactated Ringers' solution flush at 3.0 ml/s. Images were acquired at 100 frames/s, with a pullback speed of 5.0 mm/s, resulting in an image-to-image pitch of 50 μm. **(A)** A left anterior oblique angiogram after drug-eluting stent (DES) deployment shows stent site (s) **(blue arrow)** and 3.0 cm OFDI pullback segment (ps) **(red arrow)**. **(B)** Fly-through view (distal-proximal) demonstrates a calcified lesion underneath the stent **(arrow)**. **(C)** An OFDI cross-sectional image, obtained at the location of yellow arrow in B, shows a large calcific (Ca) nodule from 11-o'clock to 4-o'clock. **(D)** Perspective cutaway view of entire 3-

dimensional volume-rendered OFDI data set (left is proximal; right is distal), demonstrating the stent **(blue)**, a side branch **(yellow arrow)**, and a large calcific nodule **(red arrowhead)**. **(E)** Longitudinal section through a portion of the dataset, corresponding to the **gray dotted rectangle** in **D**. The side branch **(black arrow)** and calcific nodule **(red arrow)** are evident. Scale bar and tick marks represent 1 mm. Modified with permission from Tearney et al. (90).

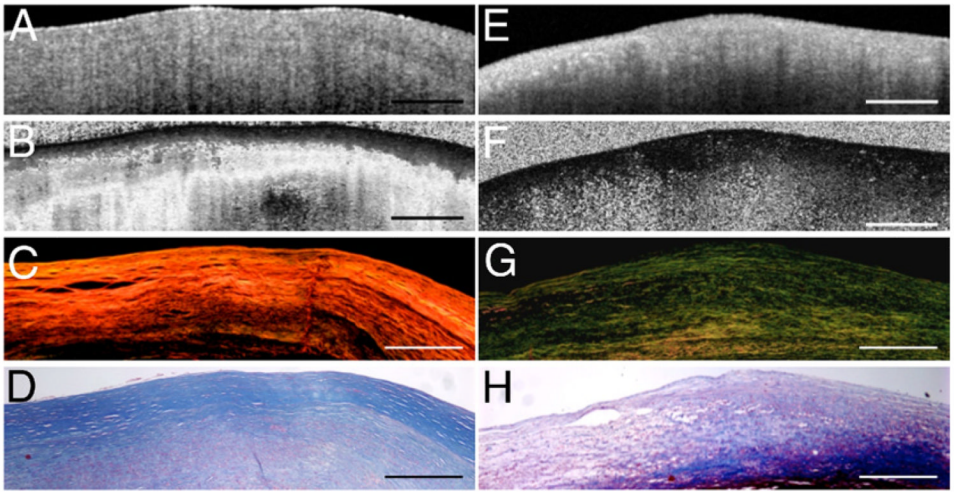

Figure 6. OCT Images and Corresponding Histopathology Demonstrating Collagen Birefringence In Atherosclerotic Plaques

(A and E) Optical coherence tomography (OCT) images of fibrous plaques. **(B)** Polarization sensitive (PS)-OCT image of the fibrous plaque in **A** showing high birefringence as seen by the rapid transition of the image from black to white, corresponding to 0° to 180° phase retardation. **(C)** Picrosirius red stained histology section showing **orange-red** fibers (thicker fibers) under polarized light microscopy. **(D and H)** Trichrome stained histology images. **(F)** PS-OCT image of fibrous plaque showing **black region** corresponding to low birefringence below the luminal surface. **(G)** Corresponding picrosirius red stained histology section showing **yellow-green** fibers (thinner fibers) under polarized light microscopy. Scale bars = 500 μm. Reprinted with permission from Nadkarni et al. (37).

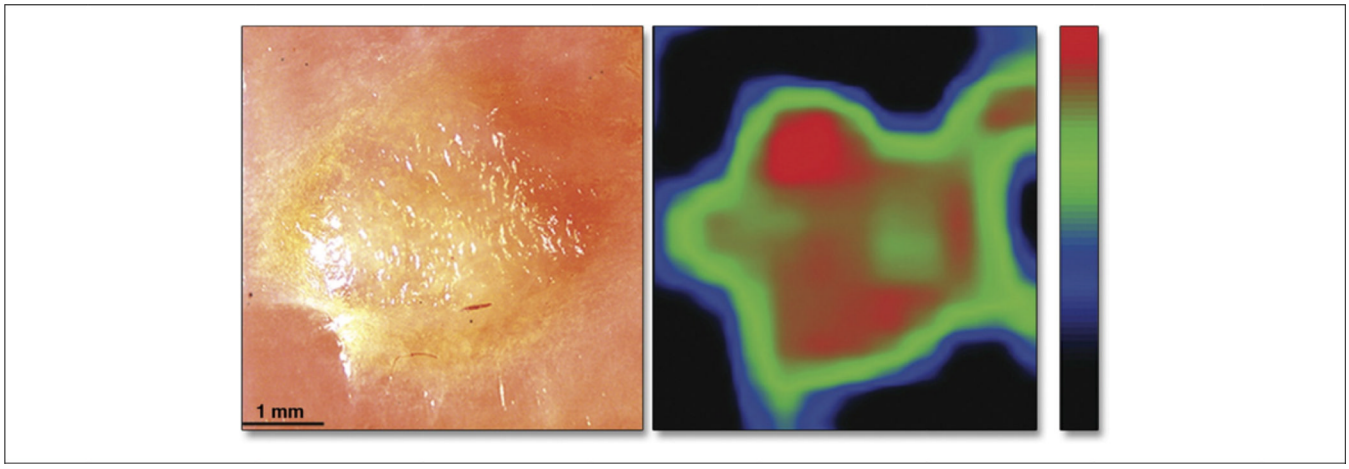

Figure 7. Cross Pathology Photograph and Spatial Distribution Map

(A) A cross pathology photograph of a lipid-rich plaque and **(B)** the corresponding spatial distribution map of the speckle decorrelation time constant (scale: **black** = 400 ms, **red** = 30 ms). The plaque borders are clearly visualized in the speckle decorrelation map in addition to regions that correspond to a reduction in cap thickness **(red regions)**. Reprinted with permission from Nadkarni et al. (38).

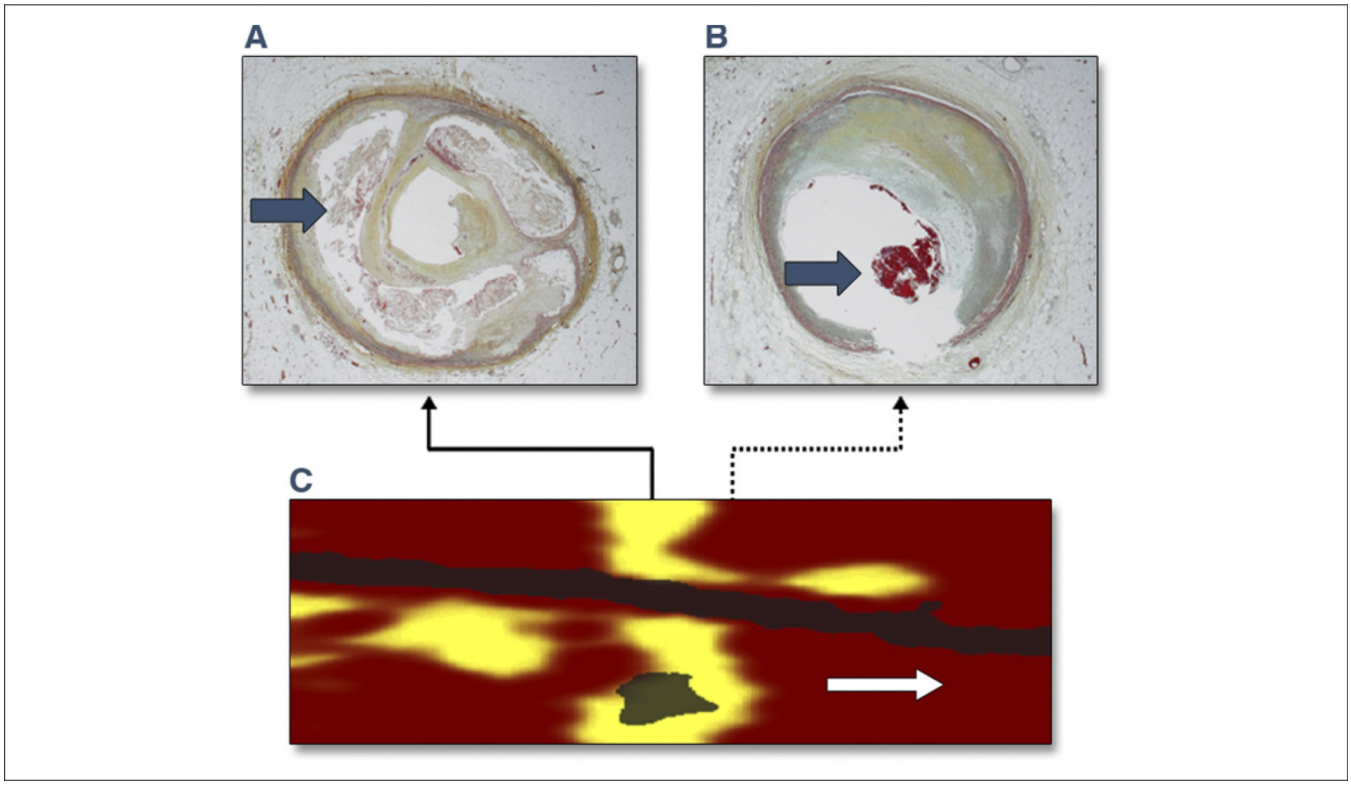

Figure 8. Circumferential Lipid-Core Plaque Histopathologic-Chemographic Correlates

(C) Near-infrared spectroscopy (NIRS) image of a large circumferential lipid-core plaque **(yellow)** imaged post-mortem. Pullback (x-axis, mm); rotation (y-axis). **(A, B)** Histological correlates from the locations indicated by the **solid arrow** and **dashed arrow** in **C**, confirming the presence of **(A)** the large lipid-core with numerous cholesterol crystals **(arrow)**, and **(B)** an intracoronary thrombus **(arrow)** at the distal edge of the lipid-core plaque. Reprinted with permission from Goldstein et al. (121).

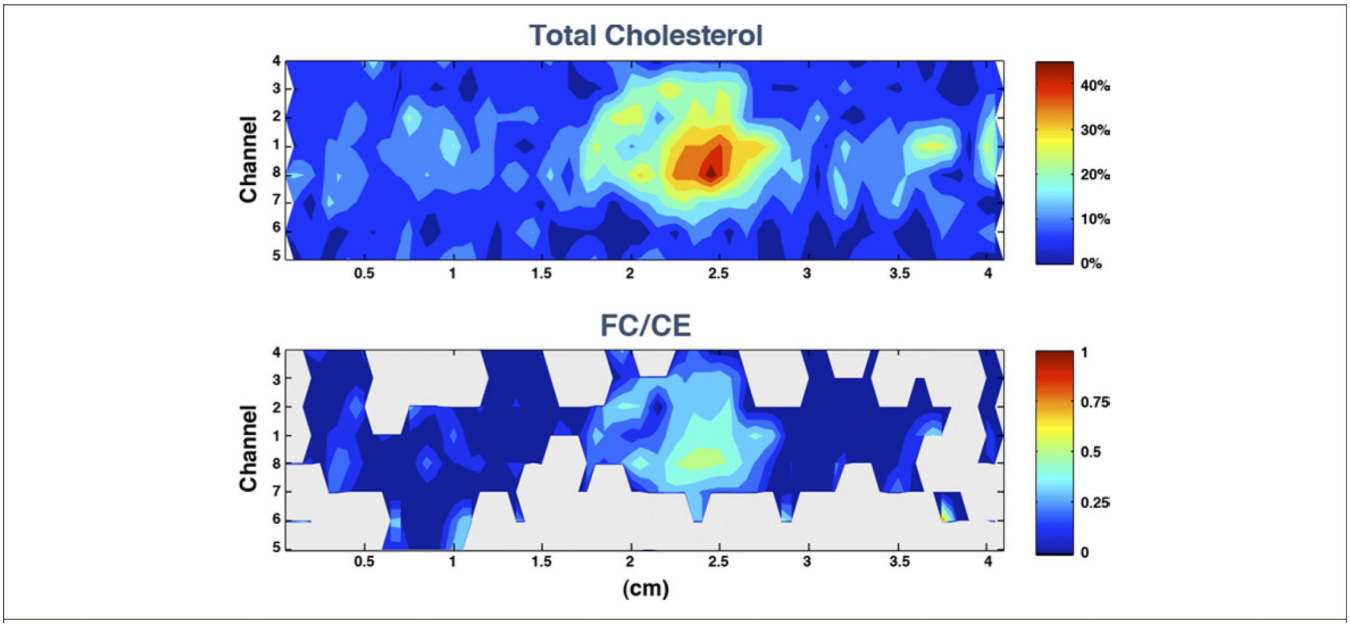

Figure 9. Chemical Concentrations Within a Human Coronary Artery Determined Using Intravascular Catheter System Based on Raman Spectroscopy

(Upper Panel) The upper contour map shows the total cholesterol concentrations throughout the artery segment. **(Lower Panel)** The lower graph displays the nonesterified-cholesterol to cholesterol ester (FC/CE) ratio, calculated when the amount of total cholesterol was estimated to be above 5% (gray otherwise). The plot abscissa indicates the length along the sample, while the ordinate indicates which fiber sensor in the catheter is recording information along a given row. The large increase in the FC content within the focal deposit centered ~2.5 cm suggests the presence of a necrotic core containing crystalline cholesterol. Figure courtesy of James Brennan.

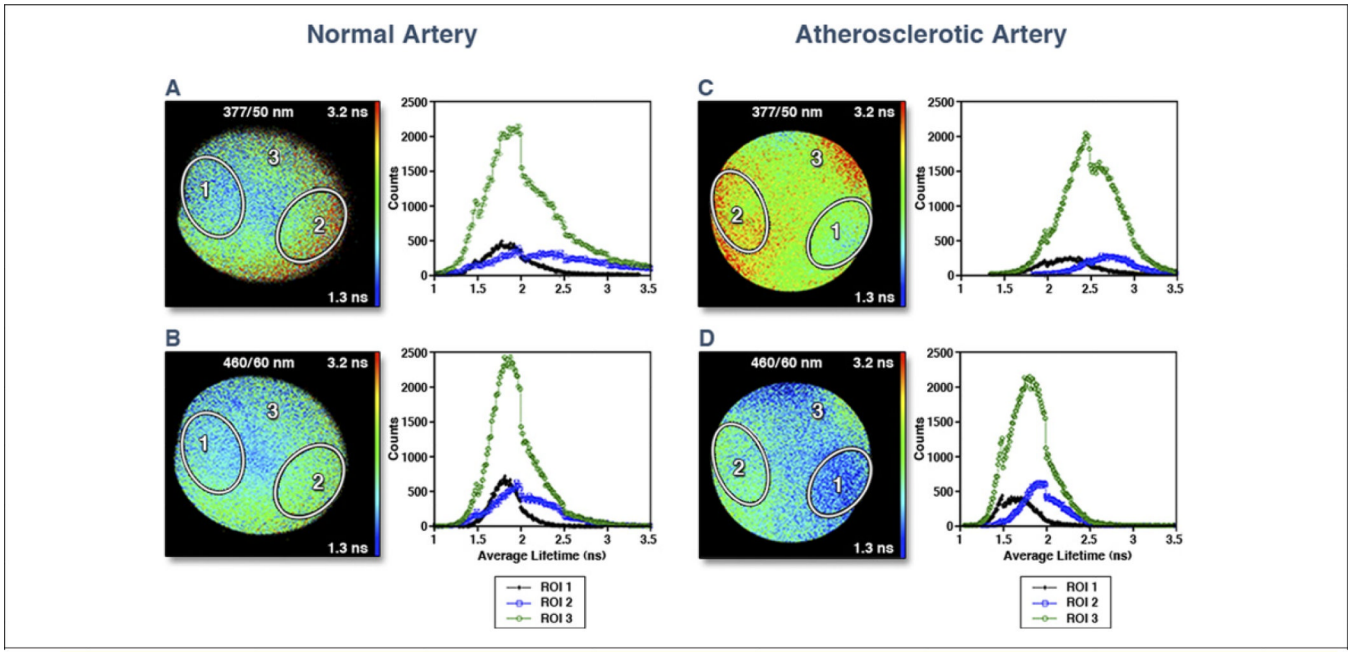

Figure 10. FLIM Images of Normal Artery

Fluorescence lifetime imaging microscopy (FLIM) images of normal artery (thoracic aorta) **(A)** at 377/50 nm (center wavelength/bandwidth) and **(B)** at 460/60 nm. Note the uniformly ~2 ns average lifetimes, characteristics of elastin fluorescence emission. Images of an atherosclerotic artery (aorta) at **(C)** 377/50 nm and at **(D)** 460/60 nm. Note the longer lifetimes in **C**, which is a characteristic of collagen fluorescence, and the shorter lifetimes in **D**, which is a characteristic of lipid fluorescence, indicating that the plaque includes both collagen-rich areas (region-of-interest [ROI] 2) and lipid-rich areas (ROI 1). Histograms depicted to the right of the FLIM images correspond to those images. **Black line** indicates ROI 1, **blue line** indicates ROI 2, and **green line** indicates ROI 3. Reprinted with permission from Marcu (142).

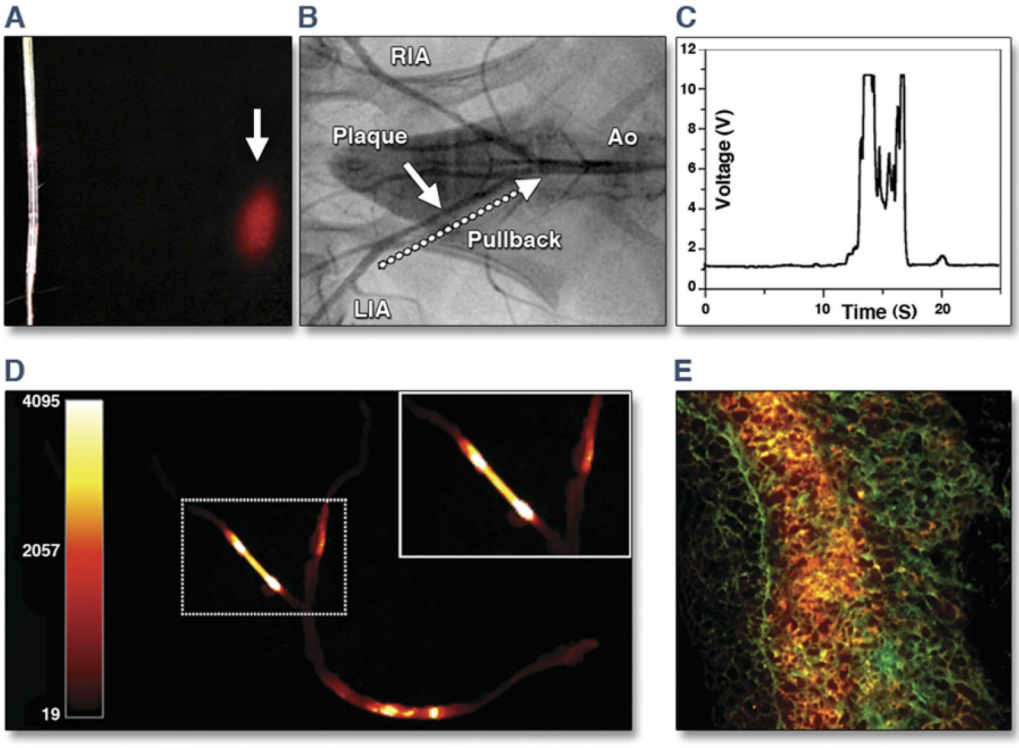

Figure 11. Real-Time Intravascular NIRF Imaging of Protease Activity

(A) The intravascular catheter was modified from a clinical optical coherence tomography guide wire used in human coronary artery imaging. Near-infrared fluorescence (NIRF) **(red)** was emitted in a 90° arc and focused 2 mm away from the aperture. **(B)** Angiogram of atherosclerotic iliac arteries after balloon injury and hyperlipidemic diet. **White arrow** indicates plaque. Twenty-four hours after Prosense750 (VisEn Medical, Woburn, Massachusetts) injection, the NIRF guide wire was placed percutaneously into the left iliac artery (LIA) and then pulled back **(dotted arrow)** manually over 20 s. Ao = aorta; RIA = right iliac artery. **(C)** Real-time voltage recordings of NIRF showed signal peaks in areas of plaques but not in control segments. **(D)** Ex vivo fluorescence reflectance images corroborated the in vivo imaging findings. **(E)** Merged 2-color fluorescence microscopy of atheroma section demonstrated focal plaque NIRF **(orange)** that was spatially distinct from 500 nm autofluorescence **(green)**. Modified with permission from Jaffer et al. (147).

Table 1

Summary of Many Key Features of Intravascular Optical Imaging Modalities Discussed, Including Mechanism, Measurement, Resolution, and Stage of Each Imaging Technology

Technology	Mechanism	Measurement	Resolution	Stage
Angioscopy	Superficial imaging	Surface structure composition	100 μm	Commercial, FDA approved
OCT/OFDI	Backscattering	Microstructure	10 μm	Commercial, FDA approved
PS-OCT	Birefringence	Collagen/SMC vs. lipid	10 μm	Pilot clinical studies
LSI	Speckle modulation	Biomechanics	100 μm	Ex vivo
NIRS	Absorption	Composition lipid	1 mm	Commercial, FDA approved
Raman	Inelastic scattering	Composition lipid	1 mm	Swine *
TR-LIFS	Autofluorescence	Composition	100 μm	Rabbit
NIRF	Fluorescence	Molecular labels	100 μm	Rabbit

* Indicates human xenograft.

FDA = Food and Drug Administration; LSI = laser speckle imaging; NIRF = near-infrared fluorescence; NIRS = near-infrared spectroscopy; OCT = optical coherence tomography; OFDI = optical frequency domain imaging; PS = polarization sensitive; SMC = smooth muscle cell; TR-LIFS = time-resolved laser-induced fluorescence spectroscopy.